筑　波　大　学

博 士 （医 学） 学 位 論 文

Functional analysis of human type 2 diabetic adipose tissue-derived mesenchymal stem cells

(2 型糖尿病患者脂肪由来間葉系幹細胞の機能解析)

2016

筑波大学大学院博士課程人間総合科学研究科

TRINH NHU THUY

Table of contents

Chapter I. General overview

1.1. Background and purposes

The prevalence of type 2 diabetes mellitus (T2DM), leading to diabetic complications, has been increasing worldwide. The possible applications of diabetic patient-derived stem cells in stem cell therapy are limited because their characteristics are still not fully understood. This study aimed to elucidate the characteristics of human type 2 diabetic adipose tissue-derived mesenchymal stem cells (dAT-MSCs) under normoxic and hypoxic conditions *in vitro* and in flap mouse model of wound healing. Furthermore, I aimed to investigate the characteristics of microvesicles isolated from human non-diabetic adipose tissue-derived mesenchymal stem cells (nAT-MSCs) and their effects on dAT-MSCs.

1.2. Materials and methods

I characterized nAT-MSCs and dAT-MSCs by fluorescence-activated cell sorting (FACS) and differentiation assay. Gene and protein expression levels were performed by quantitative reverse transcription polymerase chain reaction (qRT-PCR), Western blot, and ELISA assay. Inhibition of early growth response-1 (EGR-1) was carried out by small hairpin RNA targeted EGR-1 (shEGR-1) and treatment with PD98059 inhibitor. Chromatin immunoprecipitation (ChIP) assay was performed to find the binding of hypoxia-inducible factor-1α (HIF-1α) on EGR-1 promoter. The scratch assay and flap mouse model were used as *in vitro* and *in vivo* wound healing assays.

1.3. Results

dAT-MSCs have potential to differentiate into other cell linages and express MSC surface markers. EGR-1 and its target genes were highly expressed in dAT-MSCs in comparison to nAT-MSCs, resulting in increasing of genes and protein associated with cell adhesion, insulin resistance, and impaired wound healing in flap mouse model. Interestingly, under hypoxic conditions, HIF-1α can bind to the EGR-1 promoter in dAT-MSCs, but not in nAT-MSCs. The effects of EGR-1 were diminished by a shEGR-1 and a treatment with extracellular signal-regulated kinase 1/2 (ERK1/2) inhibitor (PD98059), suggesting that the expression of EGR-1 was upregulated in dAT-MSCs by ERK1/2 signaling pathway and HIF-1α regulation under normoxic and hypoxic conditions. Mice injected dAT-MSCs with shEGR-1 were improved their wound healing capacity.

Furthermore, I found that human nAT-MSC-derived microvesicles (nMVs) could improve dAT-MSC function by altering miRNA and mRNA expressions, which enhanced their migration ability *in vitro* and wound healing capacity in flap mouse model.

1. 4. Conclusion

dAT-MSCs increased in cell adhesion *in vitro* and impaired wound healing *in vivo*. Knockdown of EGR-1 in dAT-MSCs and the modification of nMV-treated dAT-MSCs enhance their wound healing capacity. This study suggests new therapeutic targets for improving dAT-MSC function before applying for clinical treatment.

1.5. Abbreviations

T2DM	type 2 diabetes mellitus
AT-MSCs	adipose tissue-derived mesenchymal stem cells
nAT-MSCs	AT-MSCs from non-diabetic donors
dAT-MSCs	AT-MSCs from diabetic donors
RT-PCR	reverse transcription polymerase chain reaction
SDS-PAGE	sodium dodecyl sulfate polyacrylamide gel electrophoresis
Runx2	Runt-related transcription factor 2
ALP	alkaline phosphatase
PPARγ2	peroxisome proliferator-activated receptor gamma-2
EGR-1	early growth response-1
Cyr61	Cysteine-rich angiogenic inducer 61
Col4	type IV collagen
Inαv	Integrin αv
IL6	Interleukin 6
bFGF	basic fibroblast growth factor
TGF-β	transforming growth factor beta
ERK1/2	extracellular signal-regulated kinase 1/2
AKT	a serine/threonine-specific protein kinase
SDF-1	stromal cell-derived factor 1
CXCR4	C-X-C chemokine receptor type 4
CXCR7	C-X-C chemokine receptor type 7
CCL2	chemokine (C-C motif) ligand 2
ANGPTL4	angiopoietin-like 4
nMVs	microvesicles (MVs) derived from nAT-MSCs

Chapter II. Increased expression of EGR-1 in diabetic human adipose tissue-derived mesenchymal stem cells reduces their wound healing capacity

2.1. Introduction

2.1.1. Type 2 diabetes mellitus and chronic wound

Type 2 diabetes mellitus (T2DM) has increased dramatically from 176 to 410 million people within 23 years (1990 – 2013) and become a problem worldwide [1]. T2DM is a long-term metabolic disorder that is described by high blood sugar and insulin resistance [2,3]. For temporary symptomatic treatments of T2DM, the patients undergo an intensive diet and exercise program as well as intervening with insulin or medications including metformin, acarbose or thiazolidinediones [4–6]. However, the onset of type T2DM leads to the development of the long-term consequences of microvascular and macrovascular complications [7,8].

Chronic wound, a common diabetic complication, is four times greater in diabetic patients than in non-diabetic people [9,10]. Chronic wound is a non-healing wound representing a major healthcare burden caused by delaying in wound healing process, which can be divided into four overlapping phases: coagulation and hemostasis, inflammation, proliferation, and remodeling [11,12].

2.1.2. Hypoxia regulates key factors involved in pathogenesis

Oxygen concentration in tissues is a key factor for cell and organ survival [13]. Under physiological conditions (physioxia), partial oxygen pressure (pO_2) results in the balance between oxygen delivery and its

consumption. The alteration of tissue environment leading to a decrease in pO_2 from physioxia is called hypoxia [13,14]. Hypoxic conditions have been observed in many different pathological situations like tumor development, diabetes, coronary heart disease, and transcient ischemia [13–15].

In T2DM patients, hyperglycemia and insulin resistance both seem to have important roles in the pathogenesis of diabetic complications such as chronic wound, which decrease production of trophic factors for cells and tissues as well as abnormalities in blood flow, which results in hypoxia or ischemia causing tissue disease and degeneration [7,15,16].

Hypoxia stabilizes an important transcription factor, hypoxia inducible factor (HIF)-1α. HIF-1α accumulates in the nucleus and binds to short DNA sequences near or in the promoters of target genes called hypoxia-response elements (HREs) to regulate the expression of HIF-1α target genes under hypoxic conditions [17–19]. Hypoxia-activated cell death leads to impaired endothelial cell barrier function and an increase in vascular permeability, leakage, and necrosis [14,15].

Hypoxia also increases the transcriptional activation of early growth response-1 (EGR-1) in mononuclear phagocytes and hepatoma-derived cells [20,21]. EGR-1 was first identified by Sukhatme and colleagues (1988), preferentially binds to GC-rich DNA sequences [22]. EGR-1 is rapidly and transiently expressed in the nucleus of many different cell types including endothelial cells (ECs), fibroblasts, vascular smooth muscle cells (VSMCs), monocytes, and macrophages [23–25].

2.1.3. The expression of early growth response-1 gene associated with type 2 diabetes mellitus

EGR-1 is highly expresses in the abdominal fat tissue of diabetic patients and epi fat tissue of *db/db* mice [26]. Insulin increased EGR-1 expression through activation of the extracellular signal-regulated kinase (ERK) 1/2 signaling pathway [26,27]. The increase in phosphorylation of ERK1/2 signaling elevates the expression of EGR-1, PTEN, and GGPPS leading to insulin resistance in mouse adipocytes [26,27].

EGR-1 activates the expression of many growth factors such as bFGF and TGF-β, adhesion molecules (Cyr61, ICAM-1 and MCP-1), and the inflammatory signaling cascade of TNF-α and IL-6. Thus, high EGR-1 activity is involved in the pathogenesis of atherosclerosis, restenosis, and cardiovascular diseases [23–25]. A previous study demonstrated that atherosclerosis and vascular inflammation were decreased in homozygous Egr-$1^{-/-}$/apo$E^{-/-}$ double-knockout mice [25].

2.1.4. Potencies of adipose tissue-derived mesenchymal stem cells in clinical applications

Adipose tissue-derived mesenchymal stem cells (AT-MSCs) are considered as an important potential source due to many advantages: easy isolation, abundant amount, and auto-transplantation [28–30]. Like hMSCs form other sources, AT-MSCs express hMSC surface markers and possess self-renewal capacity, long-term viability, and multilineage potential [29,30].

Earlier studies in cell-based therapies for diabetic wound healing focused mainly on fibroblasts; however, recent studies have elucidated the benefits of mesenchymal stem cells (MSCs) [31,32]. The therapeutic effect of AT-MSCs is dependent on their capacity to secrete soluble factors, including growth

factors, cytokines and chemokines that inhibit cell apoptosis, stimulate cell proliferation, promote vascularization and modulate the immune response [32–34]. It has been reported that AT-MSCs are able to stimulate proliferation, migration and matrix production of cultured dermal fibroblasts and endothelial cells via a paracrine patterns [28,34,35]. The activity of AT-MSCs in the *in vivo* wound healing appears to stimulate early inflammation response and promotes functional regeneration of the tissues by mesenchymal cells, fibroblasts, epithelial cells, and keratinocytes during the inflammation and proliferation phase [32,34,35].

Other report from my laboratory, Kimura et al. (2014) demonstrated that mice transplanted with AT-MSCs increased the degree of calcification at the joint region of bone fracture more than mice transplanted with bone marrow-derived MSCs (BM-MSCs) or dental tissue-derived MSCs (DT-MSCs). In addition, AT-MSCs showed higher ability to promote the blood flow and recruit CD45- and F4/80-positive cells in ischemic region of vascular occlusion mouse model than those of BM-MSCs and DT-MSCs [36], suggesting the high capacity of AT-MSCs in wound healing compared to BM-MSCs and DT-MSCs.

In spite of that, it has been demonstrated that dAT-MSCs have different gene expression profiles from nAT-MSCs and exhibited a low capacity for differentiating into osteoblasts and chondrocytes in comparison to nAT-MSCs under in vitro conditions that mimicked hyperglycemia [37]. The present study aimed to elucidate the characteristics of dAT-MSCs under normoxic and hypoxic conditions *in vitro* and *in vivo*, in a mouse model of wound healing, to allow for a better understanding of the potential future applications of dAT-MSCs in stem cell therapy.

2.2. Materials and methods

2.2.1. Antibodies

The following antibodies were used for the analyses of stem cell markers: Fluorescein isothiocyanate (FITC)-labeled anti-HLA-ABC (311404, BioLegend, San Diego, CA), FITC-labeled anti-CD90 (328107, BioLegend), phycoerythrin (PE)-labeled anti-CD13 (301701, BioLegend), PE-labeled anti-CD166 (559263, BD Pharmingen), PE-labeled anti-CD105 (323206, BioLegend), PE-labeled anti-CD73 (550257, BD Pharmingen), PE-labeled anti-HLA-DR (307606, BioLegend), PE–labeled anti-CD31 (303106, BioLegend), PE-labeled anti-CD14 (301806, BioLegend), allophycocyanine (APC)–labeled anti-CD45 (555485, BD Biosciences, San Jose, CA), and FITC-labeled anti-CD34 (555821, BD Biosciences). APC-labeled anti-IgG1 (555751, BD Biosciences), PE-labeled anti-IgG1 (555749, BD Biosciences), FITC-labeled anti-IgG1 (555748, BD Biosciences) were used as the isotype controls. After staining the nAT-MSCs and dAT-MSCs with fluorochrome-conjugated antibodies, the cells were sorted and analyzed using a MoFlo (MoFlo XDP; Beckman Coulter, Brea, CA).

The following primary antibodies were used for the Western blotting analyses: rabbit mAb Akt (11E7, #4685) and Phospho-Akt (Ser473) (D9E, #4060S); p44/42 ERK1/2 (137F5, #4695) and Phospho-p44/42 ERK1/2 (D13.14.4E, #4370S)**;** rabbit anti-IRS-1 (D23G12) and rabbit antibody phospho-IRS-1 (serine 636/639) (2388) (Cell Signaling Technology, Danvers, Massachusetts); rabbit anti-EGR-1 (588, sc-110); goat anti-β Actin (C-11, sc-1615); goat anti-Lamin B (M20, sc-6217) (Santa Cruz Biotechnology, Santa Cruz, CA); rabbit anti-HIF-1α (NB100-479, Novus Biologicals, Littleton, CO);

HRP-conjugated goat anti-rabbit IgG (656120) and rabbit anti-goat IgG (611620) (Invitrogen, Carlsbad, CA) were used as the secondary antibodies.

2.2.2. The isolation of AT-MSCs

The studies are performed according to the amended Declaration of Helsinki and all of the experiments were approved by the ethics committee of the University of Tsukuba. Human adipose tissue was obtained after obtaining informed consent from diabetic (n=3, HbA1c>7.0, long-term treatment) and non-diabetic (n=3) donors, male, age=59±10 years, who were undergoing procedures in the Department of Cardiovascular Surgery, University of Tsukuba Hospital, Tsukuba, Japan (Table 3). The isolation of AT-MSCs was performed as previously described [36].

Cells were cultured in Iscove's Modified Dulbecco's Medium (12200-069, Invitrogen), 10% FBS, 2 mg/mL L-glutamine (25030, Invitrogen), 5 ng/mL recombinant human bFGF (Peprotech, 064-04541, London, United Kingdom) at 37°C in 5% CO_2 and a humidified atmosphere. After 3 days, the medium containing non-adherent cells was removed and replaced with fresh medium. Frozen cell stocks were prepared using Cell Banker solution (ZENOAQ, Koriyama, Japan) and stored in liquid nitrogen for further experiments. All AT-MSCs used for the experiments of this study at passage 5−8.

2.2.3. The in vitro differentiation of AT-MSCs

In vitro differentiation was performed as described previously [36]. Osteogenic and adipogenic differentiation were assessed on day 21 by 1% Alizarin Red S (Kodak, Tokyo, Japan) and Oil Red O (Muto Pure Chemicals,

Tokyo, Japan) staining, respectively. The final step of assessing the differentiation was to measure absorbance at 482 nm and 490 nm for Alizarin Red and Oil Red O staining, respectively using a spectrophotometer Gene Quant^{TM}100, 4280 V1.6.1 (GE Healthcare, Tokyo, Japan).

To assess chondrogenic differentiation, cell pellets were sectioned and stained with hematoxylin and eosin (Muto Pure Chemicals) and Toluidine blue (Muto Pure Chemicals) to visualize the control cells and chondrocytes, respectively. The cells were visualized with an Olympus IX71 microscope (Olympus, Tokyo, Japan) under UPlan FI (×10 and ×20). All of the differentiation experiments were performed independently. The nAT-MSC and dAT-MSC experiments were performed in triplicate.

2.2.4. The cell proliferation assay

AT-MSCs were plated at a density of 4 x 10^4 cells per 35-mm dish, and cultured under normoxic (20% O_2, 37 °C) or hypoxic (5% O_2, 37 °C) conditions. The cell culture medium was replaced every 4 days. Every 24 h, the cells were washed twice with PBS and dispersed into a single cell solution using 0.05% trypsin/EDTA. The number of cells was counted using trypan blue (Invitrogen) exclusion for 10 days.

2.2.5. shRNA transfection

The shRNAs were designed for human EGR-1 (NM_001964, TRCN0000273850, Sigma-Aldrich, Louis, MO, USA). shRNA transfection was performed using hexadimethrine bromide transfection reagent (Sigma-Aldrich) according to the manufacturer's protocol.

2.2.6. Insulin stimulation

Insulin stimulation was performed as described previously [27]. nAT-MSCs and dAT-MSCs were cultured under normoxic (20% O_2, 37 °C) or hypoxic (5% O_2, 37 °C) conditions until cells reached 80% confluence. Insulin (1000 nM) was added for 1 h to allow for the detection of IRS-1 phosphorylation.

2.2.7. Analysis of ERK1/2 activity in AT-MSCs

nAT-MSCs and dAT-MSCs were cultured in normoxic (20% O_2, 37 °C) or hypoxic (5% O_2, 37 °C) conditions, until the cells reached 80% confluence. PD98059 (P215, Sigma-Aldrich), an inhibitor of ERK1/2, was used, according to the manufacturer's protocol, at a concentration 50 μM for 60 min to detect mRNA expression.

2.2.8. Quantitative RT-PCR

To examine the expression of genes related to osteogenic and adipogenic differentiation, nAT-MSCs and dAT-MSCs were assessed at day 7 after induction. nAT-MSCs and dAT-MSCs were cultured under normoxic (20% O_2, 37 °C) or hypoxic (5% O_2, 37 °C) conditions for 5 days and RNA was extracted using an RNeasy mini kit (Qiagen, Valencia, CA).

Total RNA (1 μg) was reverse transcribed using an RT-PCR kit (TOYOBO, Japan). cDNA was analyzed using a GeneAmp 7500Fast Real-Time PCR System (Life technologies) using CYBR green reagent (TOYOBO). The expression levels of the target genes were analyzed using

the ΔΔCt method. The sequences of the primer sets used for the PCR reactions are shown in Table 1.

2.2.9. Western blot

nAT-MSCs and dAT-MSCs were cultured under normoxic (20% O_2, 37 °C) or hypoxic (5% O_2, 37 °C) conditions for 4 days. Whole cell lysates were prepared with RIPA buffer (25 mM Tris, 150 mM NaCl, 1% NP-40, 1% sodium deoxycholic acid, 0.1% SDS) for 30 min and centrifuged at 15,000 rpm at 4 °C for 10 min. The collected supernatants were used for the Western blotting analyses. In each group, an equal amount of protein was electrophoresed on 8.5% sodium dodecyl sulphate–polyacrylamide (SDS-PAGE) gel and then transferred onto PVDF membranes (Immobilon-P, Millipore). The membranes were then incubated with a primary antibody as indicated. HRP-conjugated goat anti-rabbit IgG or rabbit anti-goat IgG was used as secondary antibody, and an enhanced chemiluminescence HRP substrate (Millipore) was used for detection. Goat anti-β-Actin and goat anti-Lamin B were used as the internal controls for monitoring protein loading and transfer.

2.2.10. ELISA assay

nAT-MSCs and dAT-MSCs were cultured under normoxic (20% O_2, 37 °C) or hypoxic (5% O_2, 37 °C) conditions for 4 days. Then, cells were treated with PD98059 (50 μM) in fresh culture medium (IMDM) for 60 min. The quantitative concentration of IL-6 (interleukin-6) present in cell culture supernatants was measured by IL-6 high sensitivity human ELISA kit (D6050,

R&D systems, Minneapolis, USA) following the manufacturer's protocol.

2.2.11. Chromatin immunoprecipitation (ChIP) assay

dAT-MSCs were cultured under normoxic (20% O_2, 37 °C) or hypoxic (5% O_2, 37 °C) conditions for 4 days. A ChIP assay was performed using a ChIP-IT Express Enzymatic Kit (Active Motif, Carlsbad, CA, USA) according to the manufacturer's instructions. The extracted chromatin samples were enzymatically sheared and immunoprecipitated with rabbit anti-HIF-1α, and control IgG as the primary antibodies. The precipitated genome fragments were subjected to a PCR. The PCR primer set was designed for the HRE sequence on the EGR-1 promoter as follows:

hEGR-1 -3k HRE sense (AGACTTCCACAGGCGATTCTGCTGC) and antisense –(GCAATTGGCATTCAACAAACAGTGG).

2.2.12. Animal studies

Female C57BL/6 mice were purchased from Charles River Japan, Inc. (Yokohama, Japan). All of the mice were maintained on a 12-h light/dark cycle in the Animal Research Center of the University of Tsukuba. All protocols of the protocols of the animal experiments were approved by the Animal Care Committee of the University of Tsukuba. The mouse skin flap model was performed as described previously [38]. Briefly, 10-week-old C57BL/6 mice were anesthetized and a peninsular shaped incision (3 cm × 2 cm) was made on the dorsal surface, generating an ischemia gradient by blood flow restriction. The mice were divided into 5 groups: PBS (n=5), nAT-MSC (n=30), dAT-MSC (n=30), dAT-MSC-mock (n=5), and dAT-MSC-shEGR-1 (n=6).

In each of the AT-MSC transplantation groups, cells were injected

locally on the dorsal surface at 4 positions (5 x 10^5 cells/200 μL IMDM/mouse). Immunosuppression was induced by the intraperitoneal injection of cyclosporin-A (20 mg/kg body weight; Wako, Osaka, Japan) every 2 days. The efficiency of wound healing of C57/BL6 mice with injection of cyclosporin-A was not different from that of BALB/c nu/nu mice without the cyclosporin-A treatment [69]. Therefore, C57/BL6 mice with the cyclosporin-A treatment were used in this study. After 7 days, 200 μL of Banderiraea simplicifolia-I (BS-I) lectin-TRITC (0.1 mg/mL; Sigma-Aldrich) was injected into the tail vein, approximately 30 min before sacrifice. Images of the ischemic flap were captured. The flap tissue was embedded and sectioned for analysis.

2.2.13. Histological analysis

The tissue structure and vessel formation were stained using hematoxylin and eosin counterstain and BS-I lectin-TRITC, respectively. The inflammatory cells in the ischemic tissue were examined by immunohistochemical staining with PE-labeled anti-CD45 (30F11, BD Pharmingen). Relative value of vessel per area was based on the fluorescence intensity ratio per each field and measured by Image J software (NIH, Maryland, USA). A number of CD45 cells were counted in each field. The presented data were the average of ten fields per data.

2.2.14. Statistical analysis

Student's t-test was used to determine the significance of differences between two experimental groups. The one-way ANOVA, followed by Bonferroni post-hoc test (SPSS software, IBM Corp., NY, USA), was used to

determine statistical differences among three or four experimental groups. A P-value < 0.05 was considered to indicate statistical significance. All of the data are presented as the mean ± standard deviation (SD).

2.3. Results

2.3.1. The differentiation potential and the expression of mesenchymal stem cell surface markers in nAT-MSCs and dAT-MSCs

AT-MSCs are known to possess the ability to differentiate into several types of mesenchymal cells and to express some mesenchymal stem cell markers [28–30]. In order to examine the differentiation potential of dAT-MSCs, nAT-MSCs and dAT-MSCs were cultured under conditions that would induce differentiation into osteoblasts, adipocytes, and chondrocytes. Alizarin Red, Oil Red O, and Toluidine blue staining were performed to examine calcification in osteoblasts, lipid accumulation in adipocytes, and cartilage proteoglycan synthesis in chondrocytes, respectively (Fig. 1A).

Both nAT-MSCs and dAT-MSCs had the same potential to differentiate into osteocytes and chondrocytes (Fig. 1A, 1B). On the other hand, the differentiation ability toward adipocyte lineage was higher in dAT-MSC than that in nAT-MSC. Consistent with these observations, the expression levels of the two adipocyte-specific genes (PPARγ2 [39] and adiponectin [40]) were greater in dAT-MSCs than in nAT-MSCs, whereas the expression levels of the osteogenic genes (Runx2 [41] and ALP [42]) in dAT-MSCs and nAT-MSCs were comparable (Fig. 1C).

A flow cytometric analysis revealed that the MSC-specific cell surface markers except CD166/ALCAM were expressed at similar levels in both dAT-

MSCs and nAT-MSCs (Fig. 2). CD166/ALCAM expressed higher in dAT-MSCs compared to nAT-MSCs. It has been reported that CD166/ALCAM is a close structural and functional homolog of RAGE [43], and RAGE-mediated regulation of adiposity and inflammation associated with T2DM and diabetic vascular complications [44]. Collectively, these findings demonstrate that of these two types of AT-MSCs, dAT-MSCs possess a greater potential to differentiate into adipocytes; the other phenotypes were indistinguishable from nAT-MSCs.

2.3.2. The ability to improve wound healing is impaired in dAT-MSCs in the mouse skin flap model

The proliferation activity of nAT-MSCs and dAT-MSCs were examined under normoxic and hypoxic conditions. In the log phase, the average doubling time in nAT-MSCs and dAT-MSCs was similar under both normoxic and hypoxic conditions (Fig. 3A). As expected, both types of AT-MSCs proliferated faster under hypoxic conditions. On day 7 of culture, when the cells reached confluence, the dAT-MSCs that were cultured under hypoxic conditions appeared to be difficult to dissociate into single cell suspensions by trypsinization. Even with an extended treatment time with a higher concentration of trypsin/EDTA, the number of countable dAT-MSCs was much lower due to cell aggregation (Fig. 3B).

The increased cell aggregation and adhesion of the dAT-MSCs only appeared under hypoxic conditions. I hypothesized that the increased aggregation and adhesion of dAT-MSCs might affect their regenerative activity in ischemic tissue in vivo. To test this, the wound healing activity of AT-MSCs was examined using mice with an ischemic flap. Although the

injection of both AT-MSCs improved the recovery from injury at one week after surgery, the necrotic surface area was larger in the dAT-MSC injected mice than in the nAT-MSC injected mice (Fig. 4A, 4B).

The H&E staining of the ischemic flap revealed a hypertrophic epidermis, which resembled normal wound healing, in the nAT-MSC-injected mice. In contrast, the hypertrophy of the epidermis was less evident in the dAT-MSC-injected mice (Fig. 4C). The improved wound healing of the nAT-MSC-injected mice was also shown by Lectin-TRITC staining, which shows the active neovascularization. Notably, the formation of neovascularization was less prominent in the flap in the dAT-MSC-injected mice (Fig. 4C, 4D).

At one week after surgery, the flap of the untreated mice showed significant CD45-positive cell infiltration, suggesting that the inflammation that occurred in response to tissue injury was prolonged (Fig. 4C, 4E). In contrast, the number of CD45-positive cells in the flap of the nAT-MSC-injected mice was much lower than that in the untreated mice (Fig. 4C, 4E). A greater number of CD45-positive cells were observed in the flap of the dAT-MSC-injected mice than in the nAT-MSC-injected mice (Fig. 4C, 4E). Taken together, these findings indicate the impaired ability of dAT-MSCs to improve wound healing in the ischemic flap in mouse model of ischemia.

2.3.3. The expression of EGR-1 is increased in dAT-MSCs

To explore the molecular basis for the impaired wound healing effects of dAT-MSCs, I focused on EGR-1, a zinc finger transcription factor, since the overexpression of this molecule in adipocytes has been reported to promote insulin resistance in T2DM patients [26,27]. Indeed, EGR-1 protein was more abundant in dAT-MSCs than in nAT-MSCs under both normoxic

and hypoxic conditions (Fig. 5A). A quantitative RT-PCR revealed that the mRNA level of EGR-1 was significantly greater in dAT-MSCs than in nAT-MSCs, indicating that EGR-1 was upregulated at the transcriptional level (Fig. 5B).

Although the expression of EGR-1 is known to be rapidly and transiently induced by stress signals, including hypoxia, it is noteworthy that EGR-1 was highly expressed in dAT-MSCs, even under normoxic conditions. Consistent with these observations, the mRNA levels of the two target molecules of EGR-1 in adipocytes, PTEN and GGPPS [26,27], were higher in dAT-MSCs than in nAT-MSCs. Interestingly, although the level of EGR-1 protein was comparable under normoxic and hypoxic conditions, hypoxia induced the expression of PTEN, but not GGPS1 (the gene encoding GGPPS) (Fig. 5C).

A previous study reported that the phosphorylation of insulin receptor substrate-1 (IRS-1) at Ser636 was increased in skeletal muscle cells from T2DM patients due to an increase in basal MAPK activity [45]. Since EGR-1 has been shown to augment Erk/MAPK signaling through the upregulation of PTEN and GGPPS [26,27], I examined whether the phosphorylation of Ser636/639 by IRS-1 was increased in dAT-MSCs by Western blot analysis (Fig. 5D). In the absence of insulin, I did not observe any phosphorylation of Ser636/639 of IRS-1 (data not shown). In contrast, in the presence of insulin, the phosphorylation of Ser636/639 of IRS-1 was observed in dAT-MSCs under the normoxic conditions; this phosphorylation was further increased under hypoxic conditions (Fig. 5D) (in place of the phosphorylation of IRS-1 on tyrosine sites [46,47]).

Aside from its role in insulin signaling, EGR-1 has been shown to play

multiple roles in the regulation of the inflammatory response, fibrogenesis, and cell adhesion [48–52]. Since my findings showed that the wound healing effects in the mouse skin flap model were impaired in dAT-MSCs, the mRNA level of IL-6 in dAT-MSCs was more than 25-fold higher than that in nAT-MSCs under both normoxic and hypoxic conditions, and the protein level was 4-fold higher in dAT-MSCs compared to nAT-MSCs measured by ELISA assay (Fig. 6A).

In addition, the mRNA levels of the cytokines and adhesion molecules that are known to be regulated by EGR-1 [49–52] using a quantitative RT-PCR. I found that the expression levels of EGR-1 target cytokines (bFGF and TGF-β) were significantly higher in dAT-MSCs than in nAT-MSCs under hypoxic conditions (Fig. 6B). Although the mRNA level of bFGF was observed to be increased in dAT-MSCs in comparison to nAT-MSCs, irrespective of oxygen tension, the upregulation of TGF-β in dAT-MSCs was only observed under hypoxic conditions (Fig. 6B).

Among the known EGR-1 target genes that encode cell adhesion molecules, Cyr61 and Col4 were more highly expressed in dAT-MSCs than in nAT-MSCs, irrespective of oxygen tension, whereas the increased expression of Inαv was only observed under hypoxic conditions (Fig. 6C). Collectively, these data suggest an important role of EGR-1 in regulation many target genes, which respond in insulin resistance, cell adhesion, and inflammation that may associate with the impaired wound healing activity of dAT-MSCs in vivo.

2.3.4. Activated ERK1/2 signaling is the major upstream signal of EGR-1 activation in dAT-MSCs

Although EGR-1 expression is known to be induced by hypoxia, the direct effect of HIF-1α on EGR-1 gene transcription is controversial, since hypoxia-induced EGR-1 expression is retained in hepatoma cells which lack HIF-1β (a heterodimeric partner of HIF-1α) [21]. In support of this hypothesis, the induction of HIF-1α was similarly observed in both types of AT-MSCs, despite EGR-1 expression being constitutively activated in dAT-MSCs (Fig. 7A). Interestingly, a ChIP assay revealed that, under hypoxic conditions, HIF-1α binds directly to a putative HRE within the EGR-1 promoter in dAT-MSCs, but not in nAT-MSCs (Fig. 7B).

It has been shown that EGR-1 expression is induced by various stress signals, including tissue injury, oxidative stress and hypoxia [48,50,51]. EGR-1 expression is induced through the activation of extracellular signal-regulated kinase 1/2 (ERK1/2) [53,54]. In order to determine the upstream signaling that is involved in the activation of EGR-1 in dAT-MSCs, I examined the effect of PD98059, an inhibitor of MAPK/ERK kinase, on the EGR-1 protein levels in AT-MSCs. The level of ERK1/2 phosphorylation in both types of AT-MSCs was clearly reduced by PD98059 treatment, whereas the treatment did not affect the phosphorylation of AKT at serine 473 (Fig. 8A).

EGR-1 expression was almost completely repressed by PD98059 in both types of AT-MSCs under normoxic conditions (Fig. 8B). Interestingly, however, the persistent expression of EGR-1 was detected in the PD98059-treated dAT-MSCs under hypoxic conditions, suggesting that an additional upstream signal is involved in the EGR-1 induction in dAT-MSCs under hypoxic conditions (Fig. 8B). These results indicate that the increased EGR-1

expression that is observed in dAT-MSCs under hypoxic conditions is mediated by at least two distinct mechanisms: ERK1/2 signaling activation and direct transcriptional activation by HIF-1α.

To evaluate the relative contribution of the ERK1/2 pathway in dAT-MSCs on the expression of the EGR-1 target genes, the effect of PD98059 on the expression of the EGR-1 target genes was examined by a quantitative RT-PCR (Fig. 9). In the presence of PD98059, the mRNA levels of all of the cytokines and adhesion molecules that were examined were reduced in dAT-MSCs to levels that were comparable to those in nAT-MSCs (Fig. 9).

As a result of the remarkable changes of IL6 and Cyr61 in mRNA levels, I analyzed these two proteins by Western blot and ELISA assay (Fig. 10). These data confirmed that the protein level of IL6 and Cyr61 were remarkably increased in dAT-MSCs compared to nAT-MSC. Consistent with the result in mRNA expression, the expressions of IL6 and Cyr61 were significantly decreased in dAT-MSCs the presence of the inhibitor (Fig. 10). Thus, these data suggest that the ERK1/2 pathway is the major upstream signal for the expression of EGR-1 in dAT-MSCs. On the other hand, the effect of HIF-1α on EGR-1 expression is minor, but is specifically observed in AT-MSCs under diabetic conditions.

2.3.5. The constitutive activation of EGR-1 is responsible for the impaired wound repair activity of dAT-MSCs

My findings showed that dAT-MSCs were less effective for improving wound repair in the ischemic flap and that EGR-1 expression was constitutively activated in dAT-MSCs. In order to provide direct evidence of the involvement of EGR-1 in the impaired wound healing activity of dAT-

MSCs, EGR-1 expression was knocked down by shRNA. As shown in Figure 11A, EGR-1 expression was reduced by shRNA in dAT-MSCs at both the mRNA and the protein level (Fig. 11A). In accordance with the reduction in EGR-1, the expression of Cyr61 at protein level was abolished in the knockdown EGR-1-dAT-MSCs under both normoxic and hypoxic conditions (Fig. 11B).

In addition, the expression levels of PTEN and GGPS1, three cytokines (bFGF, TGF-β, and IL-6), and three adhesion molecules (Cyr61, Col4, and Inαv) were significantly decreased under hypoxic conditions (Fig. 11C and Fig. 12). In accordance to the result in Figure 9, the gene expression levels of TGF-β, Col4, and Inαv were not affected by PD98059 in dAT-MSCs under normoxic conditions (Fig. 9). The mRNA level of PTEN, TGF-β, Col4, and Inαv was not significantly reduced by shEGR-1 under normoxic conditions in dAT-MSCs, whereas the expression levels of the other genes were comparable in both types of AT-MSCs under normoxic conditions (Fig. 12). These data suggest that the role of EGR-1 in the regulation of these genes was restricted under normoxic conditions.

2.3.6. The reduced expression of EGR-1 in dAT-MSCs promotes wound repair activity

In order to examine whether the repression of EGR-1 by shRNA restored the ability to improve wound healing in dAT-MSCs, the wound healing activity of EGR-1-deficient dAT-MSCs was examined using the mouse skin flap model (Fig. 13A). I found that the knock-down of EGR-1 in dAT-MSCs significantly reduced the necrotic surface area of the ischemic flap.

The H&E staining of the wound section showed that the epidermis of mice injected with EGR-1-deficient dAT-MSCs was thicker than that in mice that were injected with dAT-MSCs (Fig. 13B). Moreover, neovascularization was significantly increased, whereas the infiltration of CD45-positive cells was reduced in the EGR-1-deficient dAT-MSCs in comparison to the controls (Fig. 13B–D). Collectively, these data suggest that the constitutive activation of EGR-1 in dAT-MSCs is responsible for the impaired wound repairing activity. dAT-MSCs expressed excessive adhesion molecules and pro-inflammatory cytokine IL-6, which may cause prolonged inflammation phase in wound healing process (Fig. 14).

2.4. Discussion

I found the same characteristics, gene and protein expression patterns of dAT-MSCs from three diabetic donors who have similar backgrounds (gender, HbA1c, period, and treatment of T2DM). To have a good comparison between nAT-MSCs and dAT-MSCs, I also examined nAT-MSCs from three non-diabetic donors who also have comparable range of age and gender (Table 1).

My work showed that EGR-1 is constitutively activated in AT-MSCs derived from T2DM patients. I focused on this molecule because its overexpression in adipocytes plays a central role in insulin resistance in T2DM patients [26,27]. The overexpression of EGR-1 leads to the activation of two critical target genes (PTEN and GGPS1) in adipocytes. While GGPPS activates MAPK/ERK1/2 signaling, PTEN impairs PI3K/Akt signaling, thereby reducing signals from insulin receptors in T2DM adipocytes [26,27]. My data showed the increased expression of PTEN and GGPS1 and the

phosphorylation of IRS-1 at serine 636/639 in dAT-MSCs, suggesting an early manifestation of insulin resistance at the stem cell level under diabetic conditions.

My data showed that dAT-MSCs appeared to aggregate exclusively under hypoxic conditions in vitro, and that these cells were less effective for improving wound healing in the mouse skin flap model**.** The repression of EGR-1 by shRNA restored the ability of dAT-MSCs to improve wound healing, suggesting that EGR-1 is responsible for the impaired wound repair ability of dAT-MSCs (Fig. 13). Notably, the reduction of EGR-1 in dAT-MSCs significantly improved neovascularization at wound site on the ischemic flap (Fig. 13C).

Macro/microangiopathy in T2DM patients is characterized by the increased expression of a variety of growth factors and adhesion molecules [3,7]. For instance, bFGF and TGF-β are known to increase vascular permeability and coagulation, which leads to blood flow abnormalities in patients with diabetic angiopathy [7,51]. Cyr61, Col4, and Inαv are the markers of microangiopathy in diabetic patients [55–58]. In agreement with previous reports, my results showed the upregulation of these growth factors and adhesion molecules in dAT-MSCs at mRNA level (Fig. 6B, 6C).

Importantly, Cyr61 is an extracellular matrix protein and plays an important role as an angiogenic mediator. It has been reported that Cyr61 participates in the pathogenesis of proliferative diabetic retinopathy and rheumatoid arthritis [55,59]. In this study, the mRNA levels of Cyr61 was significantly decreased in both PD98059-treated dAT-MSCs and in EGR-1 knock-down dAT-MSCs (Fig. 9B, 12A). In addition, the expression of Cyr61 at protein level was diminished in dAT-MSCs treated with inhibitor or shEGR-1

(Fig. 10A, 11B).

IL-6 has been shown to play critical roles in T2DM, obesity and cardiovascular diseases [60,61]. The circulating levels of plasma IL-6 are increased in T2DM patients who are treated with insulin [60]. Excessive amounts of IL-6 have been shown to prolong the inflammatory response in injuries and to delay the wound healing process [62,63]. In fact, the expression of IL-6 in dAT-MSCs was 25-fold higher at mRNA level and 4-fold increase at protein level than in nAT-MSCs (Fig. 6A). The expression of IL6 was downregulated in the presence of PD98059 at mRNA (Fig. 9B) and protein levels (Fig. 10B). Thus, it is likely that IL-6 plays a key role in the impairment of the wound healing ability of dAT-MSCs.

Further studies are required to determine the precise roles of the individual cytokines and adhesion molecules that are highly expressed in dAT-MSCs under normal or diabetic conditions in vivo (db/db mice).

The increased expression of EGR-1 has also been reported in patients with scleroderma, an autoimmune disease that affects collagen [31]. The induction of EGR-1 by TGF-β plays an important role in the promotion of fibrosis in the fibroblasts of scleroderma patients [54]. Interestingly, in EGR-1 null mice, the impaired healing of cutaneous wounds and fibroblast-specific EGR-1 overexpression under the control of the Col1a2 promoter resulted in the robust healing of incisional wounds [38]. In contrast, the aberrant and persistent expression of EGR-1 in peripheral tissue promoted scleroderma and pulmonary fibrosis in a murine model [54,55]. Taken together with my present data, these results suggest that EGR-1 plays a dual role in wound healing which is dependent on the cellular context. Given that fibroblasts are descendants of MSCs, the biological function of EGR-1 might change with

cellular differentiation. Thus, the rigorous regulation of EGR-1 expression would be important to the appropriate control of wound healing.

Although several studies have suggested EGR-1 to be a hypoxia-inducible gene, the elevated expression of EGR-1 in dAT-MSCs was constitutively observed under both normoxic and hypoxic conditions (Fig. 5A, 5B). Since EGR-1 expression was clearly diminished by PD98059, an inhibitor of MAPK/ERK kinase ERK1/2 (Fig. 8B), MAPK signaling is likely to be the major upstream regulator of EGR-1 in dAT-MSCs. In fact, phosphorylated ERK activates ELK-1 binding to serum response elements (SRE) in EGR-1 promoter [53], indicating MAPK signaling pathway promotes mutual activation of EGR-1 expression in both AT-MSCs.

Of note, the residual expression of EGR-1 was found in dAT-MSCs under hypoxic conditions (Fig. 8B), suggesting the existence of an additional pathway of EGR-1 regulation in dAT-MSCs under hypoxic conditions. HIF-1α bound directly to the EGR-1 promoter in dAT-MSCs examined by ChIP assay, suggesting that EGR-1 expression is regulated by both MAPK signaling and HIF-1α in dAT-MSCs. This regulatory pathway of EGR-1 by HIF-1α is relatively minor; however, under certain pathological conditions, it might play a specific role in T2DM patients.

Interestingly, although the EGR-1 protein levels were similar under normoxic and hypoxic conditions, EGR-1 shRNA treatment resulted in the reduction of a group of genes (TGF-β, Col4, and Inαv) under hypoxic, but not normoxic conditions (Fig. 9). Consistently, PD98059 only affected the expression of these genes under hypoxic conditions (Fig. 9). These results suggest that the expression of these genes is only regulated by EGR-1 under hypoxic conditions. The molecular mechanism underlying the functional

differences of EGR-1 under normoxic and hypoxic conditions remains to be elucidated.

In conclusion, the present study demonstrates that the expression of EGR-1 was upregulated in dAT-MSCs through two different pathways. The main regulatory pathway is the MAPK/ERK pathway, which is independent of oxygen tension. The other regulatory pathway is mediated by HIF-1α through the direct transcriptional activation at the promoter region of the EGR1 gene. The latter is observed under hypoxic conditions in dAT-MSCs but not in nAT-MSCs. My data demonstrate that a high level of EGR-1 is responsible for the impaired wound healing effect of dAT-MSCs. Thus, the control of EGR-1 expression by the manipulation of the upstream MAPK/ERK signaling and HIF factors could be a new therapeutic target for stem cell therapy in T2DM patients with chronic wounds and tissue ischemia.

Chapter III. Microvesicles enhance the mobility of human diabetic adipose tissue-derived mesenchymal stem cells in vitro and improve wound healing in vivo

3.1. Introduction

3.1.1. Mesenchymal stem cells and microvesicles

AT-MSCs secrete supportive soluble factors enhance cellular communication, allowing information delivery from one cell to another by a paracrine signaling, which is prerequisite of a rapid cellular and tissue response [28–30]. Recent studies suggested that cellular communication has also involved intercellular transfer of extracellular vesicles including exosomes and microvesicles (MVs), which released by cells during apoptosis or stimulation [64,65]. Healthy cells can bud MVs directly from their plasma membrane (100 – 1000 nm in diameter), which contain a lot of genetic information from secreting cells [64–66]. MSCs release MVs associated with cell-to-cell communication and the ability of switching the cell function of recipient cells [66,67].

3.1.2. Mesenchymal stem cells-derived microvesicles (MSC-MVs) are considered as a potential therapeutic tool in clinical application

MSC-MVs deliver bioactive cargo and specific microRNAs, mRNAs, and proteins to recipient cells to induce phenotypic, epigenetic, and functional changes in the recipient cells that promote the activation of regenerative programs in somatic cells such as hepatic cells, fibroblasts, tubular cells, and endothelial cells [68–71]. Previous reports in preclinical investigation of MSC-MVs mainly emphasized their therapeutic potential in improving the function of

renal tubular cells, modulating T cell response in patients with type 1 diabetes mellitus, reducing severe pneumonia in mice, enhancing survival in a lethal model of acute kidney injury, and inhibiting tumor cell growth [68–72].

Most reports have characterized healthy AT-MSCs, which can secrete efficient soluble factors and MVs, supporting tissue repair and regeneration [35,36,67]. By contrast, I demonstrated that dAT-MSCs have impaired function in wound healing ability due to the up-regulation of adhesion molecules and prolonged inflammatory stage. Thus, the aim of this work is to investigate how to improve the function of dAT-MSCs in wound healing and examine the effect of human AT-MSC-derived MVs on dAT-MSCs.

3.2. Materials and methods

3.2.1. The isolation of AT-MSCs

AT-MSCs were isolated using previous described protocol. Briefly, human adipose tissue was obtained after obtaining informed consent from diabetic patients (n=5, HbA1c > 7.0, long-term treatment) and non-diabetic donors (n=5, male, age=59 ± 10 years), who were undergoing procedures in the Department of Cardiovascular Surgery, University of Tsukuba Hospital, Tsukuba, Japan. All AT-MSCs used for the experiments of this study were at passage 5-8.

3.2.2. Microvesicles isolation and transfection

MVs were obtained from the supernatant of nAT-MSCs following a previous protocol [73]. Briefly, the medium of subconfluent nAT-MSCs was changed to Dulbecco's modified eagle medium (DMEM) no phenol red

(Gibco, NY, USA) containing 0.25% bovine albumin fraction (Sigma-Aldrich, Louis, MO, USA). After 24 h, the supernatants were collected and centrifuged at 1000xg for 20 min. Cell-free supernatants were ultracentrifuged at 100,000xg for 70 min at 4°C, washed with phosphate-buffer saline (PBS), and underwent second ultracentrifuge at the same conditions. MSC-surface markers on MVs were sorted and analyzed using a MoFlo system (MoFlo XDP; Beckman Coulter, CA, USA) for PE-labeled anti-CD105 (323206, BioLegend, CA, USA), FITC-labeled anti-CD90 (328107, BioLegend), and allophycocyanin (APC)-labeled anti-CD45 (555485, BD Biosciences, CA, USA). The protein content of MVs was quantified using the Bradford method (BioRad, CA, USA).

3.2.3. PKH26-labelled microvesicles

The PKH26 red fluorescent cell linker kit for general cell membrane labeling (PKH26GL-1KT, 100M0612, Sigma-Aldrich) was used to stain nAT-MSC-derived MVs according to the manufacturer's protocol. The labeled MVs were incubated with dAT-MSCs in culture (7.5 μg per 500,000 cells). The efficiency of MV-transfected cells was determined by a FACS analysis according to the red fluorescence signal after 12 h of MV transfection.

3.2.4. *In vitro* wound healing assay (scratch assay)

An in vitro scratch assay was performed according to a protocol described previously [74]. Briefly, nAT-MSCs or dAT-MSCs were seeded at a density of 3×10^5 cells per 4-well plates. After 24 h, confluent monolayers were treated with mitomycin C (10 μg/mL) for 3 h to eliminate the possibility

of cell proliferation [75]. A scratch was created with a p1000 pipet (1 mm width) and cells were non-treated or treated with MVs in the culture medium. Images of the scratch were captured at 0 h and 16 h. The analysis of the scratch area was performed using the WimScratch software program (https://mywim.wimasis.com). The data presented are the average of ten measurements from five independent scratch areas.

3.2.5. RT-PCR for miRNAs

The quantification of miRNAs using the TaqMan miRNA assays protocol (Applied Biosystems, CA, USA) was performed by two-step RT-PCR following the manufacturer's protocol. Briefly, the RT step was performed using the TaqMan miRNA reverse transcription kit (1502183, Applied Biosystems) and the PCR step was performed using TaqMan universal PCR master mix II, with UNG (1503029, Applied Biosystems) . The primers for miRNAs include hsa-miR-150 (P140506-007 F11), hsa-miR-29c (P141106-000 G07), and RNU48 (P141013-007 E07) (Applied Biosystems).

3.2.6. Quantitative RT-PCR

To examine the gene expression, RNA was extracted using an RNeasy mini kit (Qiagen, Valencia, CA). Total RNA (1 μg) was reverse transcribed using an RT-PCR kit (TOYOBO, Japan). cDNA was analyzed using a GeneAmp 7500Fast Real-Time PCR System (Applied Biosystems) using CYBR green reagent (TOYOBO). The expression levels of the target

genes were analyzed using the ΔΔCt method. The sequences of the primer sets used for the PCR reactions were in Table 1.

3.2.7. Animal studies

Female C57BL/6 mice were purchased from Charles River Japan, Inc. All of the mice were maintained on a 12-h light/dark cycle in the Animal Research Center of the University of Tsukuba. All protocols of the animal experiments were approved by the Animal Care Committee of the University of Tsukuba. The mouse skin flap model was performed as described previously. The mice were divided into 4 groups: PBS (n=5), nAT-MSC (n=10), dAT-MSC (n=10), and MV-treated dAT-MSCs (n=10).

3.2.8. Histological analysis

The tissue structure was stained by hematoxylin and eosin counterstain. Inflammatory cells in the ischemic tissue were examined by immunohistochemical staining with PE-labeled anti-CD45 (30F11, BD Pharmingen, USA). The number of CD45-positive cells was counted in each field. The presented data are the average of ten fields per section.

3.2.9. Statistical analysis

Student's t-test and one-way ANOVA (Bonferroni post-hoc test; SPSS® software, IBM Corp.) were used to determine the significant difference between two and more experimental groups, respectively. A P-value < 0.05 was considered to be statistically significanct. The data are presented as the mean ± standard deviation (SD).

3.3. Results

3.3.1. The impairment of dAT-MSCs in gene expression and migration ability in vitro

I previously demonstrated that the wound healing ability of human dAT-MSCs was impaired in the ischemic flap mouse model because of increasing numbers of adhesion molecules and a prolonged inflammation stage. In this study, I investigated the migration ability and migratory factors expressed in dAT-MSCs compared with those in nAT-MSCs. It has been reported that migration factors (SDF-1, CXCR4), survival factor (CXCR7), early response inflammatory cytokine (CCL2) and angiogenic factor (ANGPTL4) are the main soluble factors secreted from MSCs that contribute to enhanced cell proliferation, migration and survival of tumor cells and play important roles in augmenting acute and chronic wound healing [36,76,77]. Thus, I investigated these factors and found that SDF-1, CXCR4, CXCR7, CCL2, and ANGPL4 were significantly down-regulated in dAT-MSCs compared to nAT-MSCs (SDF-1, 1.9 ± 0.3 fold decrease, $P < 0.05$, n=3 in each; CXCR4, 2.2 ± 0.4 fold decrease, $P < 0.05$, n=3 in each; CXCR7, 3.5 ± 0.3 fold decrease, $P < 0.01$, n=3 in each; CCL2, 3.0 ± 0.9 fold decrease, $P < 0.05$, n=3 in each; ANGPL4, 2.0 ± 0.5 fold decrease, $P < 0.05$, n=3 in each) (Fig. 15).

I speculated that the reduction of these factors in dAT-MSCs might affect the impairment of the migration rate of dAT-MSCs. Therefore, I performed the in vitro scratch assay, a suitable method for studying the effects of cell-matrix and cell-cell interactions, which mimics cell migration during wound healing in vivo. The results showed that the percentage of

uncovered wound areas at 16 h of dAT-MSCs was remarkably higher than that of nAT-MSCs (wound area: dAT-MSCs, 19.7% ± 4.5% vs. nAT-MSCs, 10.1% ± 5.1%; $P < 0.05$, n=10 in each) (Fig. 16), indicating that dAT-MSCs had an impaired ability to migrate to the wound site, possibly due to defect in the secretion of effective factors that support this process.

3.3.2. nAT-MSC-derived MVs modify the expression of miRNAs and mRNAs in dAT-MSCs

MVs have been isolated from many sources of adult MSCs, such as the bone marrow and Wharton's jelly-MSCs [67,78]. Here, I isolated MVs from human nAT-MSCs (nMVs). I characterized nMV-surface markers by FACS and showed that nMVs expressed CD105 and CD90, but not CD45 (Fig. 17A). To examine and quantify the efficiency of nMV internalization into dAT-MSCs, I labeled nMVs with PKH26 red fluorescence [73]. After 12 h of transfection, the internalization of nMVs into dAT-MSCs was determined by PKH26 red fluorescence captured by microscopy (Fig. 17B) and quantified by FACS analysis (Fig. 17C), resulting in the generation of dAT-MSC-transfected nMVs.

MVs contain many miRNAs, which are non-coding single-stranded RNA of approximately 22 nucleotides involved in mRNA silencing and post-transcriptional regulation of the gene expression [67]. I found that miR29c and miR150 were highly expressed in dAT-MSCs compared with nAT-MSCs ($P < 0.01$, n=3 in each) (Fig. 18A). Interestingly, the expression of miR29c and miR150 was significantly down-regulated in nMV-treated dAT-MSCs compared with non-treated dAT-MSCs ($P < 0.01$, n=3 in each), suggesting that the expression of miRNA29c and miR150 were possibly alternated in

response to endogenous modification after MV internalization.

Moreover, I found that the expression of SDF-1, CXCR4, CXCR7, CCL2, and ANGPTL4 in nMV-treated dAT-MSCs was significantly elevated compared with control dAT-MSCs (SDF-1, 2.0 ± 0.4 fold increase, $P < 0.05$, n=3 in each; CXCR4, 2.1 ± 0.5 fold increase, $P < 0.05$, n=3 in each; CXCR7, 2.4 ± 0.6 fold increase, $P < 0.05$, n=3 in each; CCL2, 2.7 ± 0.6 fold increase, $P < 0.05$, n=3 in each; and ANGPL4, 3.2 ± 0.2 fold increase, $P < 0.01$, n=3 in each). Notably, the mRNA expressions of these factors in nMV-treated dAT-MSCs were at similar levels to those in nAT-MSCs (Fig. 18B, 18C).

3.3.3. nMVs enhance the wound healing ability of dAT-MSCs in vitro.

Since I found the up-regulation of soluble factors involved in the wound healing process in nMV-treated dAT-MSCs (Fig. 18B, 18C), I next examined the ability of these cells in wound healing in vitro. My data showed that the percentage of uncovered wound areas at 16 h of nMV-treated dAT-MSCs was significantly decreased compared with that of dAT-MSCs (wound area: nMV-treated dAT-MSCs, 9.3% ± 5.0% vs. dAT-MSCs, 19.8% ± 4.8%, $P < 0.01$, n=10 in each) (Fig. 19A, 19B), suggesting the migration ability of dAT-MSCs was enhanced after nMV internalization. Importantly, the migration ability of nMV-treated dAT-MSCs was similar to that of nAT-MSCs (Fig. 19A, 19B). Collectively, nMVs were able to enhance the migration rate of dAT-MSCs.

3.3.4. MV-treated dAT-MSCs improve the wound healing ability in the flap mouse model

I hypothesized that nMV-treated dAT-MSCs had increased migration and chemotaxis, supporting their regenerative activity, in ischemic tissue in

vivo. To test this hypothesis, the wound healing activity of AT-MSCs was examined using ischemic moue flap models. After one week of surgery and a subcutaneous injection of AT-MSCs, the necrotic area was significantly reduced in mice injected with nMV-treated dAT-MSCs compared with mice injected with non–treated dAT-MSCs (necrotic area: nMV-treated dAT-MSCs, 15.8% ± 3.0% vs. dAT-MSCs, 37.1% ± 8.0%, $P < 0.01$, n=10 in each) (Fig. 20A, 20B). Notably, the percentage of the necrotic area was not significant different between nAT-MSC and nMV-treated dAT-MSC injected mice (necrotic area: nAT-MSCs, 17.6% ± 5.0% vs. nMV-treated dAT-MSCs, 15.8% ± 3.0%, $P < 0.01$, n=10 in each) (Fig. 20B).

H&E staining showed recovery of the wound area and epidermis in mice injected with nMV-treated dAT-MSCs as well as nAT-MSC, whereas the wound area and epidermis were not recovered in mice injected with PBS or dAT-MSCs (Fig. 21A). Mice injected with nMV-treated dAT-MSCs or nAT-MSCs showed significantly increased frequencies of CD45-positive cells at the wound sites compared to mice injected with dAT-MSCs ($P < 0.05$, n=10) (Fig. 21A, 21B), suggesting that early inflammation occurred in response to tissue injury at day 3 of the wound healing process. These findings suggest that nMV-treated dAT-MSCs improved wound healing ability in flap mouse model.

3.4. Discussion

AT-MSCs have been shown to be efficacious in the treatment of wounds, including chronic wound [28]. However, in this study, the down-regulation of genes related to cell migration and chemotaxis was found in dAT-MSCs from five diabetic donors compared to those of nAT-MSCs from

five non-diabetic donors (Table 1), indicated reduction of the dAT-MSC function in stimulating cell migration, survival, and angiogenesis in target stromal cells. I also demonstrated that dAT-MSCs have impaired cell migration in vitro via the scratch assay (Fig. 16). Previous work has demonstrated that MVs derived from Alde-low endothelial progenitor cells (EPCs) can improve the migration and angiogenesis of non-function Alde-high EPCs [73]. I thus hypothesized that MVs from nAT-MSCs can improve the function of dAT-MSCs in wound healing.

MVs are released from various cell types including platelets, endothelial cells, erythrocytes, monocytes, lymphocytes, and leucocytes upon activation or apoptosis [64,65]. MVs derived from EPCs and MSCs improve the migration, survival, and angiogenesis of non-functioning EPCs, epithelial cells, inflammatory cells, and diabetic chronic wound fibroblasts [68–73]. MVs have the ability to act as autocrine and paracrine effectors in cell-to-cell communication due to the composition of biological materials from their parental cells, which includes bioactive lipids, integrins, cytokines, enzymes, mRNA, miRNAs, and transcription factors [64–67].

I herein demonstrated that MVs alter the expression of miR29c and miR150 in dAT-MSCs (Fig. 18A). It has been reported that miR29c and miR150 are highly up-regulated in skeletal muscles of rat type 2 diabetes mellitus by a microarray analysis [79]. On the other hand, the inhibition of miR29c can improve insulin sensitivity, while the knockdown of miR150 augments the CXCR4 expression and mobilization of bone marrow-derived mononuclear cells (BM-MNCs) [79–81]. In agreement with these reports, I found that miR29c and miR150 were highly expressed in dAT-MSCs and down-regulated after transfecting nMVs into dAT-MSCs (Fig. 18A). Previous

report identified that the expression of miR-150 was down-regulated in BM-MNCs in response to myocardial ischemia with simultaneous induction of the CXCR4 protein expression [81]. Willeit et al. (2013) also demonstrated that plasma levels of miRNAs, such as miR-126, miR-150, miR-191, and miR-223 were decreased in response to antiplatelet therapy [82], Therefore, miR29c and miR150 may have been down-regulated in nMV-treated dAT-MSCs in response to interactions within the microenvironment, leading to endogenous modification and tissue regeneration.

nAT-MSC-derived MVs have a beneficial effect on dAT-MSCs in that they can improve the expression of genes related to cell migration (SDF-1/CXCR4), survival (CXCR7), inflammation (CCL2), and angiogenesis (ANGPTL4) (Fig. 18B, 18C). Homing of MSCs to injured tissues is dependent on their ability to migrate and interact with the local microenvironment. The interaction of SDF-1/CXCR4 plays a crucial role in stem cell mobilization and improves neovascularization in vivo [77].

It has been reported that CXCR7, a survival factor, is highly expressed in AT-MSCs and promotes glioblastoma multiforme (GBM) proliferation. Knockdown of CXCR7 in AT-MSCs promoted tumor cell apoptosis due to the inhibition of the SDF-1/CXCR7 pathway in GBM [33]. CCL2 plays an important role in the early inflammation response in ischemic tissues [36], while ANGPTL4 is a crucial angiogenic factor that contributes to diabetic wound healing [76]. The triggering of these factors by nMVs may induce cell migration in wound healing *in vitro* (Fig. 19), suggesting that nMVs play a key role in intercellular modification and represent a delivery system for effective transfer of biological information to dAT-MSCs.

The wound healing capacity in the flap mouse model was impaired in

dAT-MSCs and enhanced in nMV-treated dAT-MSCs. The necrotic area was reduced in nMV-treated dAT-MSCs due to the recovery in the wound and epidermis area and the recruitment of inflammatory cells, suggesting modification of the dAT-MSC function in wound healing. Although I found the great potential of nMVs and its influence on dAT-MSCs, further studies are necessary to elucidate the mechanisms by which nMVs are able to modify the miRNA expression and manipulate gene expression in dAT-MSCs.

In conclusion, this study demonstrated that nAT-MSC-derived MVs have the ability to alter the expression of miRNA29c and miR150 and up-regulate the gene expression of SDF-1, CXCR4, CXCR7, CCL2, and ANGPTL4, which are known to play crucial roles in acute and chronic wounding. The modification of nMV-treated dAT-MSCs enhances their mobility to the wound site both in vitro and in vivo, thereby suggesting a new therapeutic target for improving the dAT-MSC function before application in clinical treatment.

Chapter IV. Conclusions and perspectives

4.1. Conclusions

In this study, dAT-MSCs have potential to differentiate into osteoblasts, adipocytes, and chondrocytes as well as expressing stem cell surface markers. Interestingly, the adipogenic differentiation was higher in dAT-MSCs than in nAT-MSCs. The expression of activated leukocyte cell adhesion molecule CD166/ALCAM is dramatically increased in dAT-MSCs compared with nAT-MSCs by FACS analysis, suggesting that this molecule may associate with the increase of adiposity and inflammation related with T2DM and its complication.

In dAT-MSCs, EGR-1 significantly elevated the expression of many target genes correlated with insulin resistance, adhesive phenomenon *in vitro*, and impairment of wound healing activity *in vivo*. EGR-1 was a key regulator, which was upregulated by ERK1/2 signaling pathway and HIF-1a in dAT-MSCs under normoxic and hypoxic conditions. The ERK1/2 inhibitor (PD98059) and knock-down of EGR-1 expression were useful to modulate the expression EGR-1 target genes and improved wound healing capacity of dAT-MSCs.

Microvesicles derived from nAT-MSCs (nMVs) expressed MSC surface markers and easy internalized into dAT-MSCs. nMVs alternated miRNA expression and modification gene expressions related to migration and chemotaxis in dAT-MSCs. By these effects, nMVs induced cell migration ability of dAT-MSCs *in vitro* and improved wound healing ability *in vivo*.

4.2. Perspectives

In perspective, EGR-1 may be an ideal therapeutic target for improving the function of dAT-MSCs before their therapeutic application. Interrupting the expression of EGR-1 in dAT-MSCs may be a useful treatment for chronic wounds in diabetic patients. The control of EGR-1 expression by the manipulation of the upstream MAPK/ERK signaling and HIF factors could be a new therapeutic target for stem cell therapy in T2DM patients with chronic wounds and tissue ischemia.

This study also demonstrates a promising opportunity to modify the function of dAT-MSCs for therapeutic stem cell application in diabetic patients. nMVs play a key role in cell communication, intercellular modification, and represent a delivery system for effective transfer of biological information to dAT-MSCs. It is a new therapeutic target for improving the dAT-MSC function before application in clinical treatment.

Tables

Table 1. The background information of adipose tissues from diabetic and non-diabetic donors

Donner #	Age	Sex	HbA1c	T1/2DM	Period (yr)	Treatment of DM
dAT#1	67	M	7.2	T2DM	20	Insulin; Novo-Rapid(12-8-10-6)
dAT#2	45	M	7.0	T2DM	7	miglitol (alpha-glucosidase inhibitor)(50) 0.5T 1X、Metformin (Biganide)(250) 3T 2X
dAT#3	39	M	7.1	T2DM	5 or more?	Insulin; Novo-Rapid(6-6-6-4). Untreated DM over several years. Insulin was induced 3 months before surgery.
dAT#4	73	M	7.0	T2DM	20	Gliclazide (Sulfonylurea)(40) 1T 1X、Metformin (Biganide)(250) 2T 2X
dAT#5	71	M	11.8	T2DM	10 or more?	untreated DM over 10 years. Blood glucose: 471 mg/dl. Body weight loss: -15 kg/2 years due to diabetes. Insulin was first induced one month before surgery.
nAT#1	70	M	5.5	none	none	none
nAT#2	66	M	5.5	none	none	none
nAT#3	69	M	5.2	none	none	none
nAT#4	67	M	4.9	none	none	none
nAT#5	44	M	4.5	none	none	none

Table 2. The primers used for quantitative polymerase chain reaction

Function	Gene	Primer	Sequence
Internal control	β-actin	5'-primer	GTGCGTGACATTAAGGAGAAGCTGTGC
		3'-primer	GTACTTGCGCTCAGGAGGAGCAATGAT
Transcription factors	EGR-1	5'-primer	AGTCTTTTCCTGACATCTCTCTGAA
		3'-primer	ACTAGGCCACTGACCAAGCTGAA
Migration factors	SDF-1	5'-primer	AACGCCAAGGTCGTGGTCGTGCTGG
		3'-primer	CTACAATCTGAAGGGCACAGTTTGG
	CXCR4	5'-primer	CTGTGACCGCTTCTAC CCCAATGACTT
		3'-primer	CCAAGGAAAGCATAGAGGATGGGGTTC
	CXCR7	5'-primer	TAAATATATGCCAGTCTTGGCTGA
		3'-primer	TTACAAAGCAGTTTTCGTTCCATA
Angiogenic factors	TGF-β	5'-primer	AGAGCTCCGAGAAGCGGTACCTGAACCC
		3'-primer	GTTGATGTCCACTTGCAGTGTGTTATCC
	bFGF	5'-primer	AGAGCGACCCTCACATCAAGCTACAAC
		3'-primer	ATAGCTTTCTGCCCAGGTCCTGTTTTG
	ANGPTL4	5'-primer	CTCAAGGCTCAGAACAGCAGGATCC
		3'-primer	CTTGGCCACCTCATGGTCTAGGTGC
Adhesion molecules	Cyr61	5'-primer	TGGGTCTGTGACGAGGATAGTATCAAGG
		3'-primer	CTTGTAAAGGGTTGTATCGGATGCGAGG
	Col4	5'-primer	AGGGCCAGCCTGGCCTGCCAGGACTTCC
		3'-primer	TCACCCTTAGAGCCTGTGATTCCTGGAG
	Inav	5'-primer	ATACGACCCCAATGTTTACAGCATCAAG
		3'-primer	GCCAGTAAAATTGTATAAGGAGGACATG
Inflammatory cytokine	IL-6	5'-primer	ACAAGAGTAACATGTGTGAAAGCAG
		3'-primer	TATACCTCAAACTCCAAAAGACCAG
	CCL2	5'-primer	ATGAAAGTCTCTGCCGCCCTTCTGTG
		3'-primer	TCAAGTCTTCGGAGTTTGGGTTTGCTT
Adipogenic markers	PPARγ2	5'-primer	GCCAAGGCTTCATGACAAGGGAGTTTC
		3'-primer	CACGTGTTCCGTGACAATCTGTCTGAG
	Adiponectin	5'-primer	CCTGGTGAGAAGGGTGAGAAAGGAGATCC

		3’-primer	TGTGATGTGGTAGGCAAAGTAGTACAGCC
Osteogenic markers	Runx2	5’-primer	CAGATGGGACTGTGGTTACTGTCATGG
		3’-primer	CCTAAATCACTGAGGCGGTCAGAGAAC
	ALP	5’-primer	ACGTGGCTAAGAATGTCATC
		3’-primer	CTGGTAGGCGATGTCCTTA
Mediators of insulin resistance	PTEN	5’-primer	TTG GCG GTG TCA TAA TGT CT
		3’-primer	GCA GAA AGA CTT GAA GGC GTA
	GGPS1	5’-primer	ACTGTTTGGATTAGCAGTAGGTCTC
		3’-primer	GGAGTGTAGATTAGCATAATCATCC

Figures and Legends

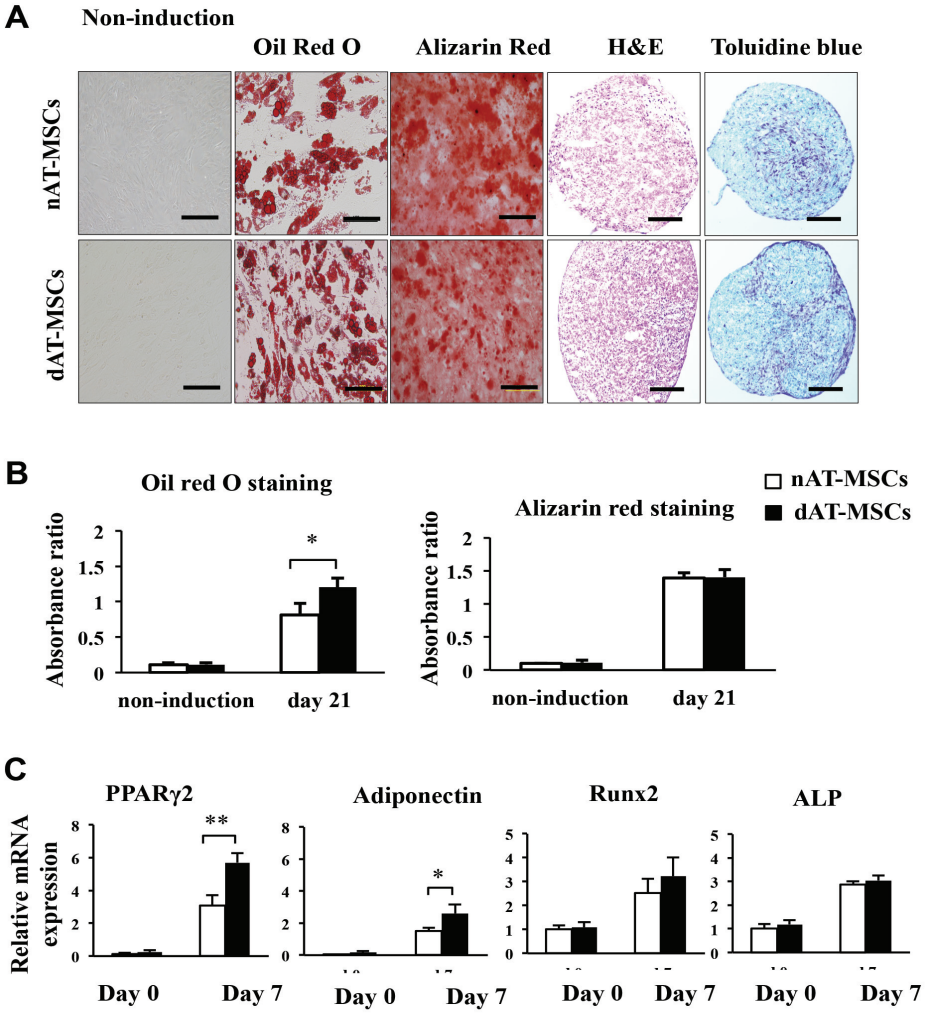

Fig. 1. Differentiation potential of dAT-MSCs in comparison of nAT-MSCs. **A,** Differentiated cells were recognized on day 21 using Alizarin Red staining, which indicated the calcification of the surface of osteoblasts (red). Oil Red O staining indicated the lipid accumulation of adipocytes (red); hematoxylin and eosin staining was performed as a control. Toluidine blue staining indicated cartilage proteoglycan and glycosaminoglycan (purple). **B,** Absorbance was measured at 482 nm and 490 nm for Alizarin Red and Oil Red O staining, respectively. In the Oil Red O staining of dAT-MSCs, absorbance was significantly higher than that in nAT-MSCs. **C,** The expression levels of differentiated master genes Runx2, ALP, PPARγ2, and adiponectin were examined by a qRT-PCR and normalized to β-actin on days 0 and 7 of osteogenic and adipogenic induction. The white and black bars indicate nAT-MSCs and dAT-MSCs, respectively. The data represent the average of three independent experiments (mean ± SD); *, $P < 0.05$; **, $P < 0.01$.

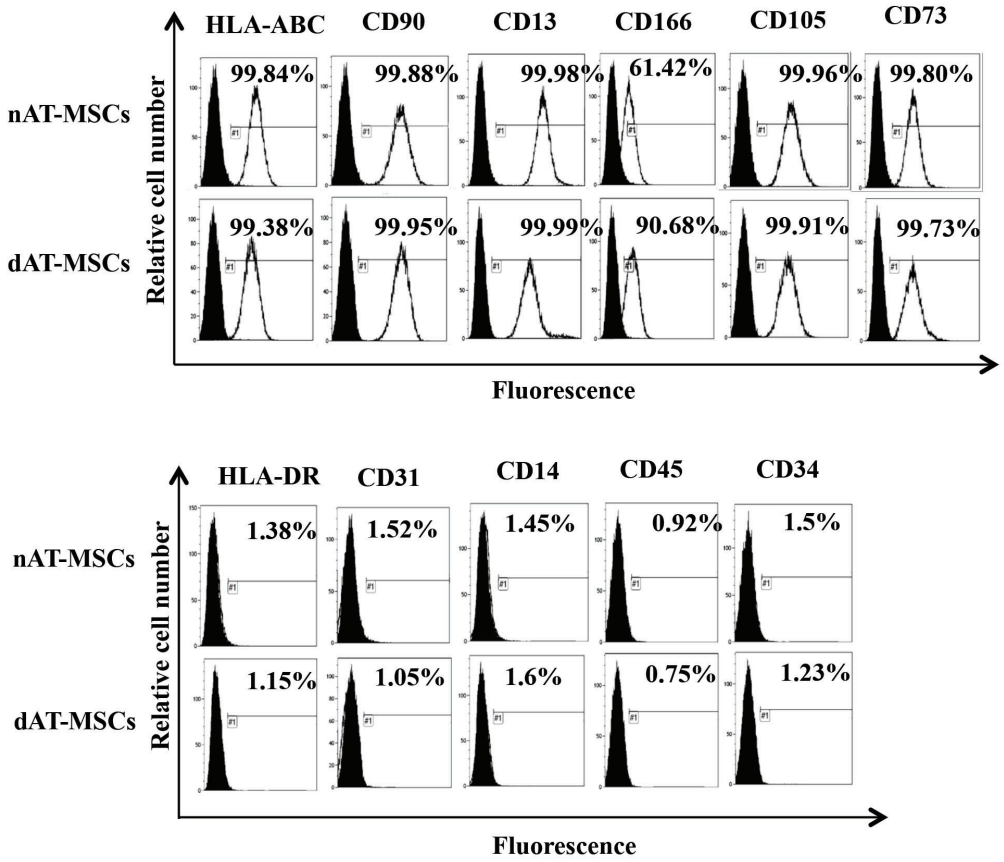

Fig. 2. nAT-MSCs and dAT-MSCs were analyzed and sorted by a FACS Vantage SE to determine the expressions of HLA-ABC, CD90, CD13, CD166, CD105, CD73, HLA-DR, CD31, CD14, CD45, and CD34 (line peaks) in comparison to isotype controls (black peaks)

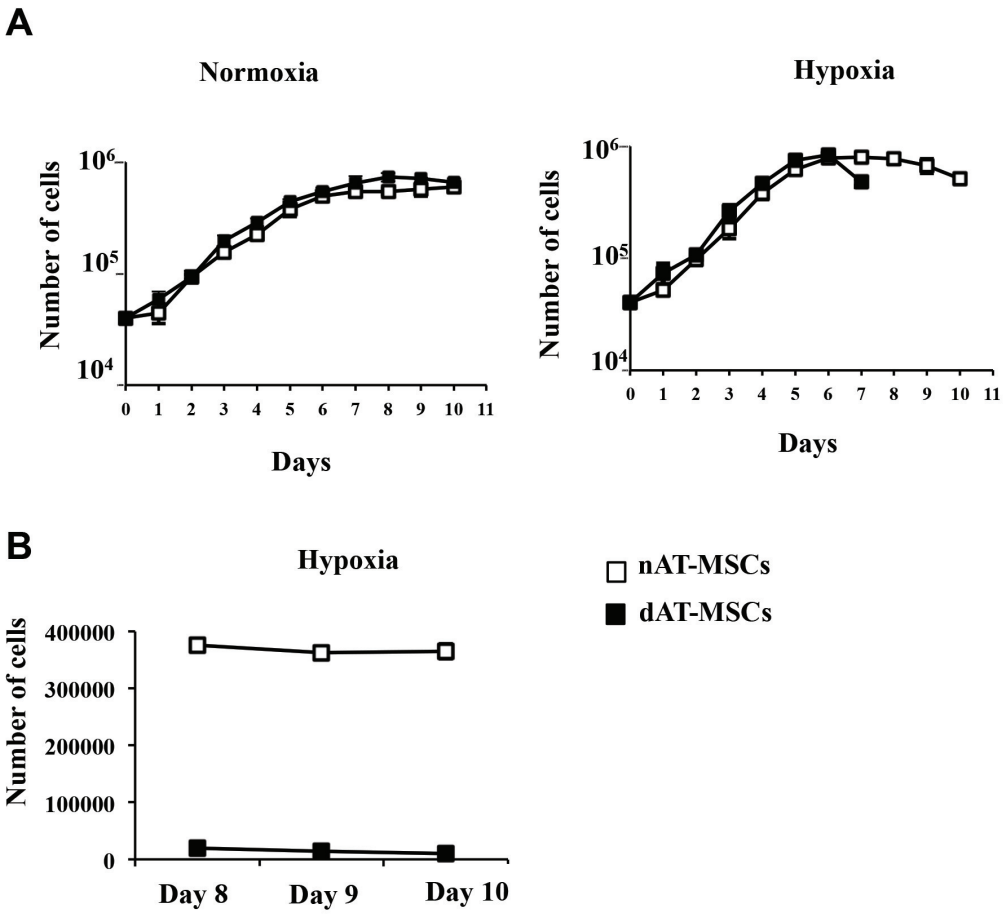

Fig. 3. Cell proliferation of nAT-MSCs and dAT-MSCs under normoxic and hypoxic conditions. A, The number of cells was counted every 24 h using trypan blue exclusion over 10 days under normoxic (20% O_2) or hypoxic (5% O_2) conditions. Abnormal cell adhesion was observed in dAT-MSCs under hypoxic conditions on day 7. The precise number of cells could not counted because the cells adhered together too tightly. The average doubling time was 32.5 ± 2 h under normoxic conditions and 28.5 ± 2 h under hypoxic conditions ($P < 0.01$). **B,** The number of dAT-MSCs was counted after abnormal cell adhesion and compared to the number of nAT-MSCs on days 8, 9, and 10.

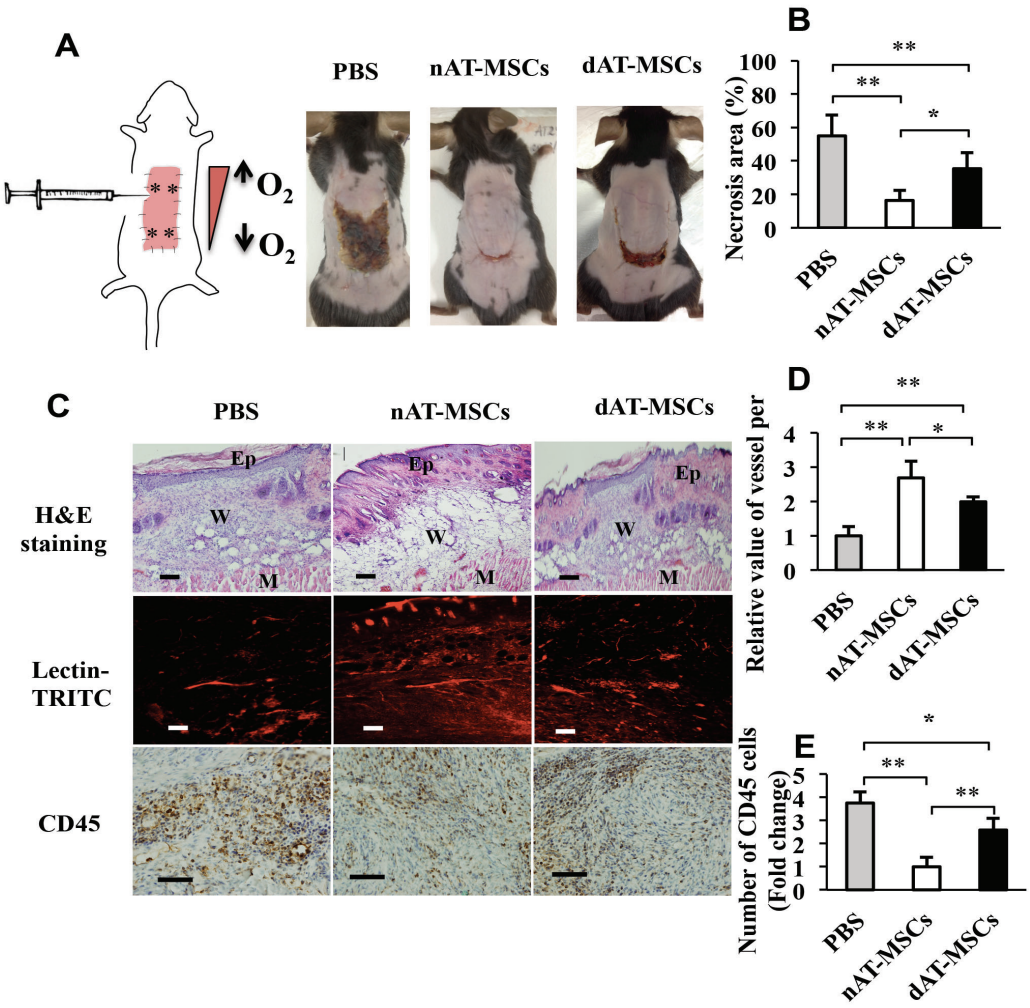

Fig. 4. dAT-MSCs were impaired in wound healing of ischemic flap mouse model. A, A flap model was created and the images of the necrotic areas of mice injected with PBS, nAT-MSCs, and dAT-MSCs were captured on day 7 after injection. **B,** The percentage of the necrotic area was calculated based on the necrotic area per wound area in mice that were injected with PBS (n = 5), nAT-MSCs (n = 30), and dAT-MSCs (n = 30). **C,** The embedded sections were examined by hematoxylin and eosin staining for tissue structure, which revealed the epidermis, wound, and muscle in each wound site; BS-I Lectin-TRITC was injected into the tail vein to observe the vessel formation (red) with fluorescence intensity; and the CD45 immunohistochemical staining of inflammatory cells (brown). **D,** The fluorescence intensity was measured using the Image J software program to evaluate the number of vessels in each area (n = 20). **E,** The CD45-positive cells were counted and expressed relative to the number nAT-MSCs (n = 10). The data represent the average of three independent experiments (mean ± SD); *, $P < 0.05$; **, $P < 0.01$. Scale bars: 100 μm; Ep, epidermis; W, wound; M, muscle.

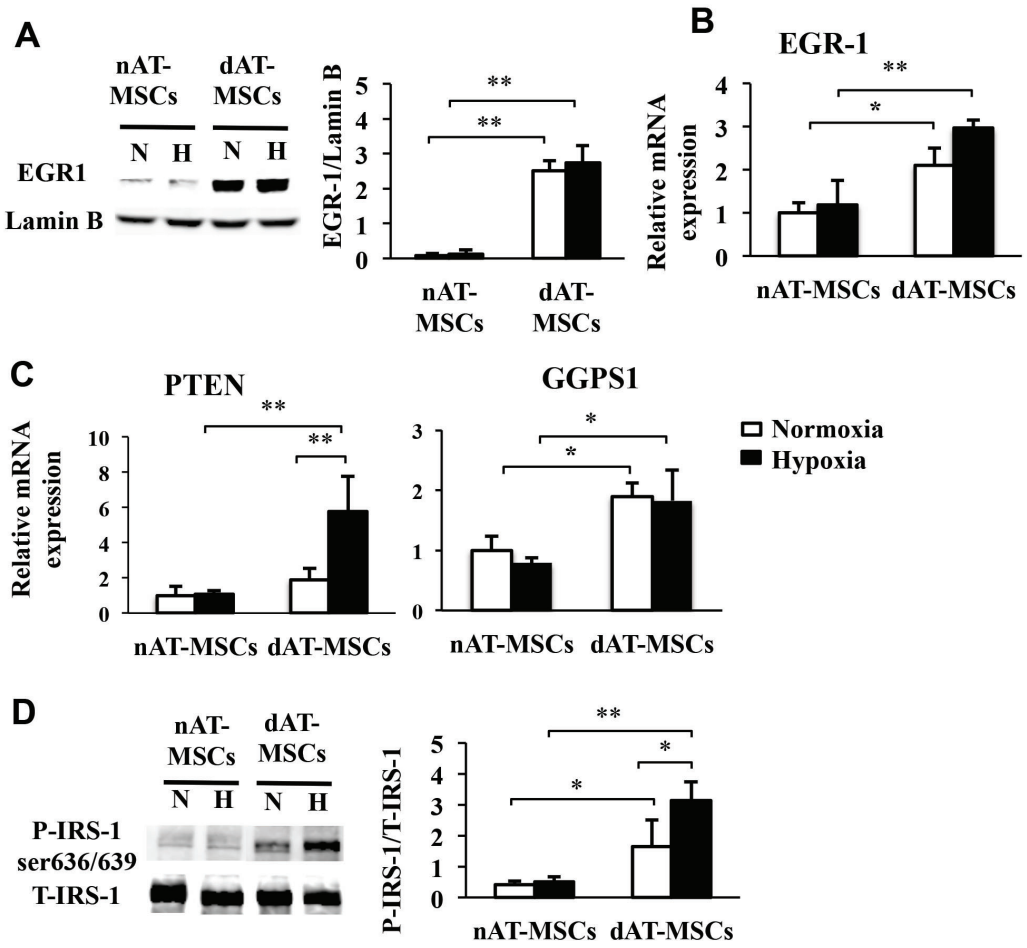

Fig. 5. dAT-MSCs highly expressed EGR-1 and increased gene expressions and phosphorylation of IRS-1 (ser636/639) associated with insulin resistance. nAT-MSCs and dAT-MSCs were cultured under normoxic (20% O_2) or hypoxic (5% O_2) conditions. **A and B**. The mRNA **(A)** and protein levels **(B)** of transcription factor EGR-1 were examined by a qRT-PCR and an immunoblot analysis, respectively normalized to β-actin and Lamin B. **C,** PTEN and GGPS1 expression was determined by a qRT-PCR and normalized to β-actin. **D,** Insulin (1000nM) was added to the culture medium for 60 min to stimulate the phosphorylation of IRS-1 (P-IRS-1). P-IRS-1 at serine 636/639 and total IRS-1 (T-IRS-1) were analyzed by immunoblotting. White and black bars indicate normoxic and hypoxic conditions, respectively. The data represent the averages of three independent experiments (mean ± SD); *, $P < 0.05$, **, $P < 0.01$. N, normoxia; H, hypoxia.

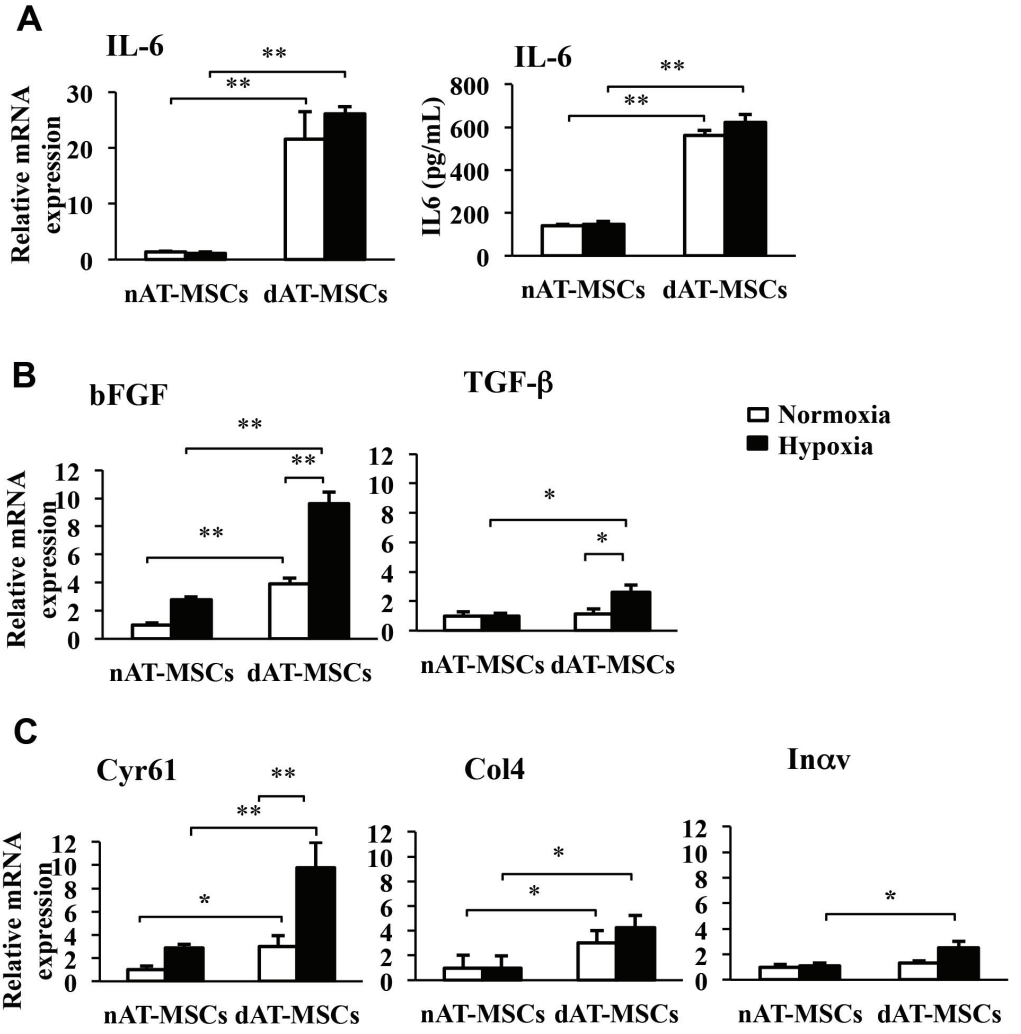

Fig. 6. Upregulation of pro-inflammatory cytokine IL-6, growth factors and adhesion molecules in dAT-MSCs. A, The mRNA expression level of IL6 was assessed by a qRT-PCR and normalized to β-actin and the quantitative protein concentration of IL-6 present in cell culture supernatants was measured by interleukin-6 (IL-6) high sensitivity human ELISA kit (D6050, R&D systems). **B and C,** The mRNA expression levels were assessed by a qRT-PCR and normalized to β-actin to determine the expression of bFGF and TGF-β **(B)**; Cyr61, Col4, and Inαv **(C)**. White and black bars indicate normoxic and hypoxic conditions, reαααααααααspectively. The data represent the averages of three independent experiments (mean ± SD); *, $P < 0.05$, **, $P < 0.01$.

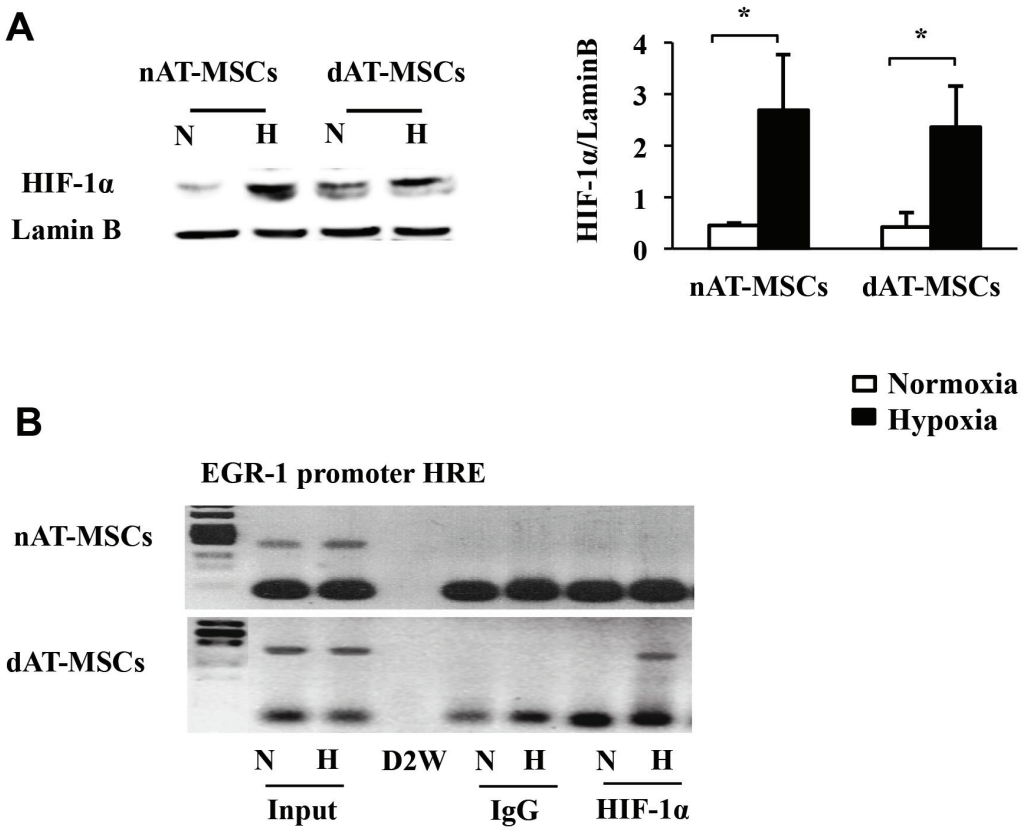

Fig. 7. HIF-1α directly regulated EGR-1 expression under hypoxic condition. **A,** HIF-1α expression was assessed in nAT-MSCs and dAT-MSCs under normoxic and hypoxic conditions by an immunoblot analysis and normalized to Lamin B. **B,** A chromatin immunoprecipitation (ChIP) assay was performed for the EGR-1 promoter HRE using an anti-HIF-1α antibody under normoxic (20% O_2) and hypoxic (5% O_2, 4 days) conditions. Input samples (1/10 input) were used as an internal control; IgG was used as a negative control. The binding of HIF-1α to the EGR-1 promoter was specified in dAT-MSCs under hypoxic conditions. The data shown are the averages of three independent experiments (mean ± SD). *, $P < 0.05$; **, $P < 0.01$. N, normoxia; H, hypoxia.

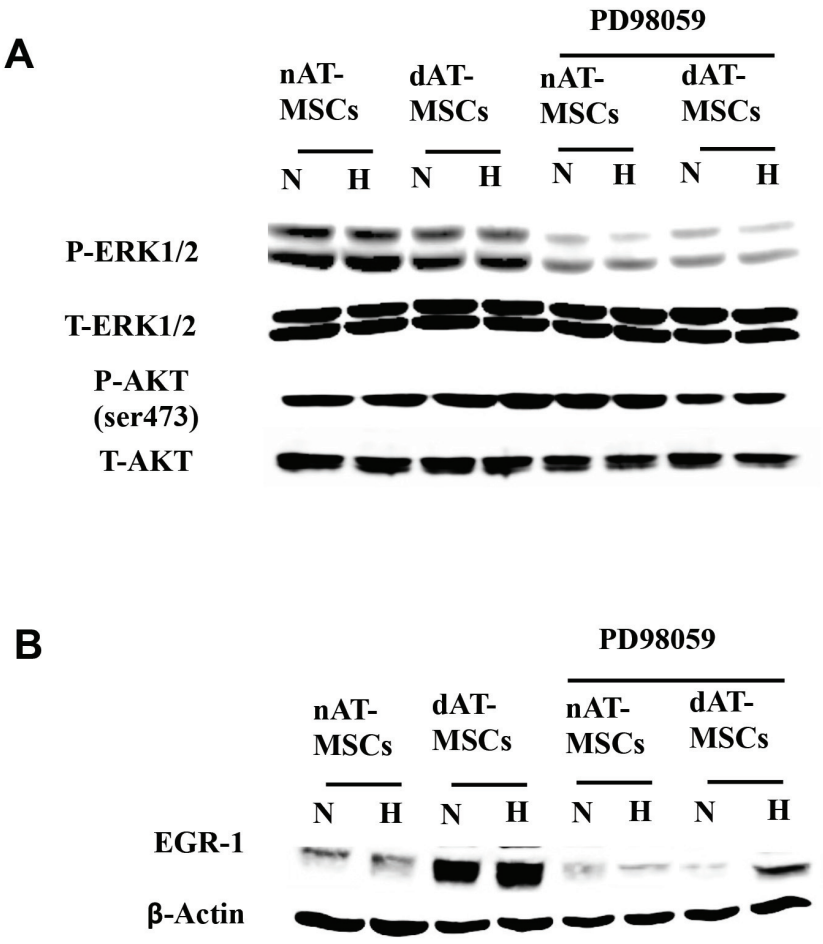

Fig. 8. PD98059 inhibited phosphorylation of ERK1/2 and EGR-1 expression. PD98059 (50 μM) was added to nAT-MSC and dAT-MSC cultures for 60 min that were maintained under normoxic (20% O_2) or hypoxic (5% O_2) conditions. Whole cell proteins were prepared for an immunoblot analysis. **A,** The phosphorylation of ERK1/2, and total ERK1/2 (T-ERK1/2), the phosphorylation of AKT at serine 473, and total AKT (T-AKT) were examined in treated and untreated cells under normoxic and hypoxic conditions. **B,** The expression levels of EGR-1 and internal control β-Actin were also assessed by immunoblotting in treated and untreated cells under nomoxic and hypoxic conditions. N, normoxia; H, hypoxia.

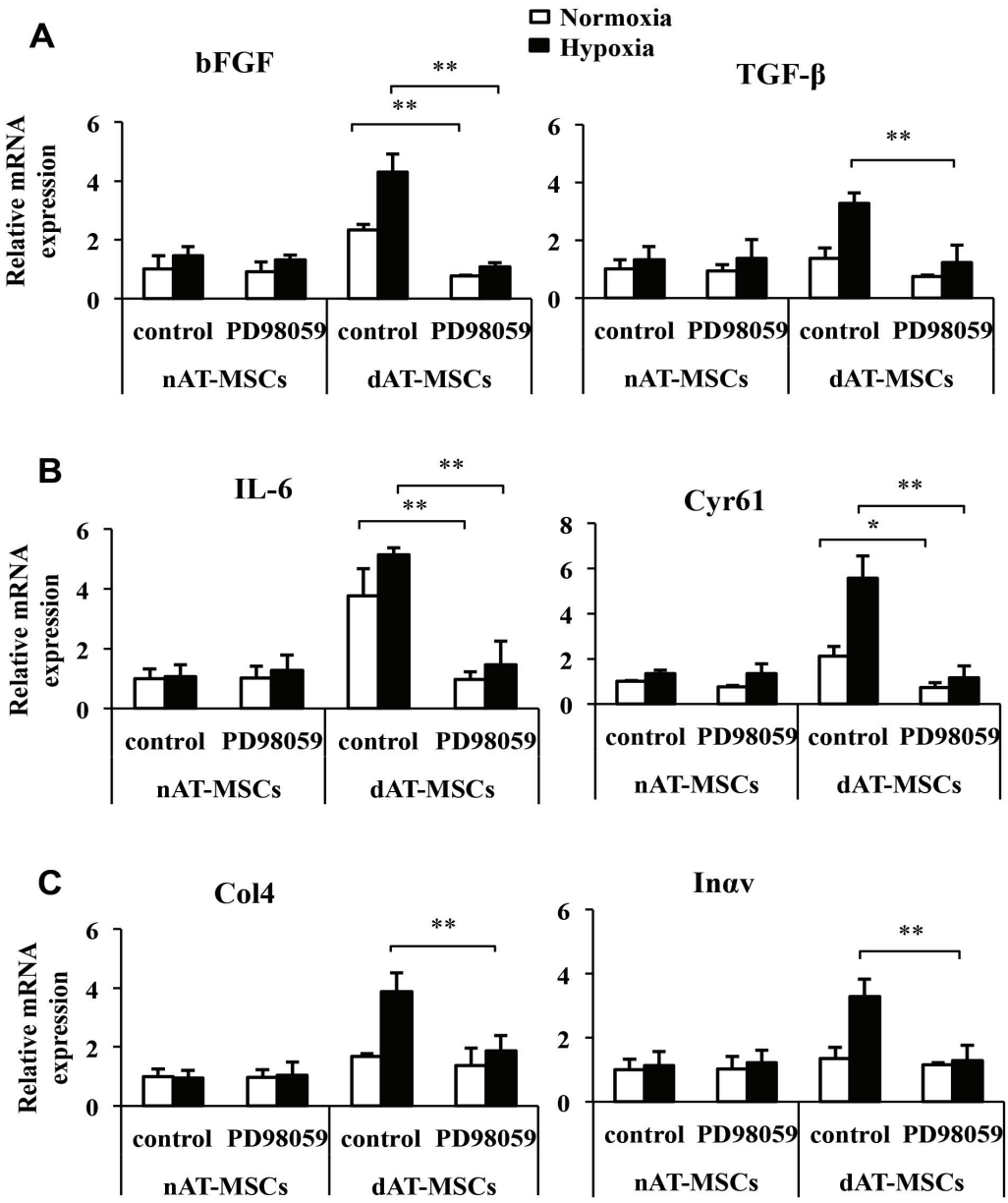

Fig. 9. The expression levels of genes related to cell proliferation, inflammation, and adhesion were down-regulated in dAT-MSCs treated with inhibitor. PD98059 (50 μM) was added to nAT-MSC and dAT-MSC cultures for 60 min that were maintained under normoxic (20% O_2) or hypoxic (5% O_2) conditions. **A – C**, The mRNA expression levels of the EGR-1 target genes were examined by a qRT-PCR and normalized to β-Actin including bFGF and TGF-β **(A)**; IL-6, and Cyr61 **(B)**; Col4 and Inαv **(C).** Controls representative for non-treated cells. The data shown are the averages of three independent experiments (mean ± SD). *, $P < 0.05$; **, $P < 0.01$.

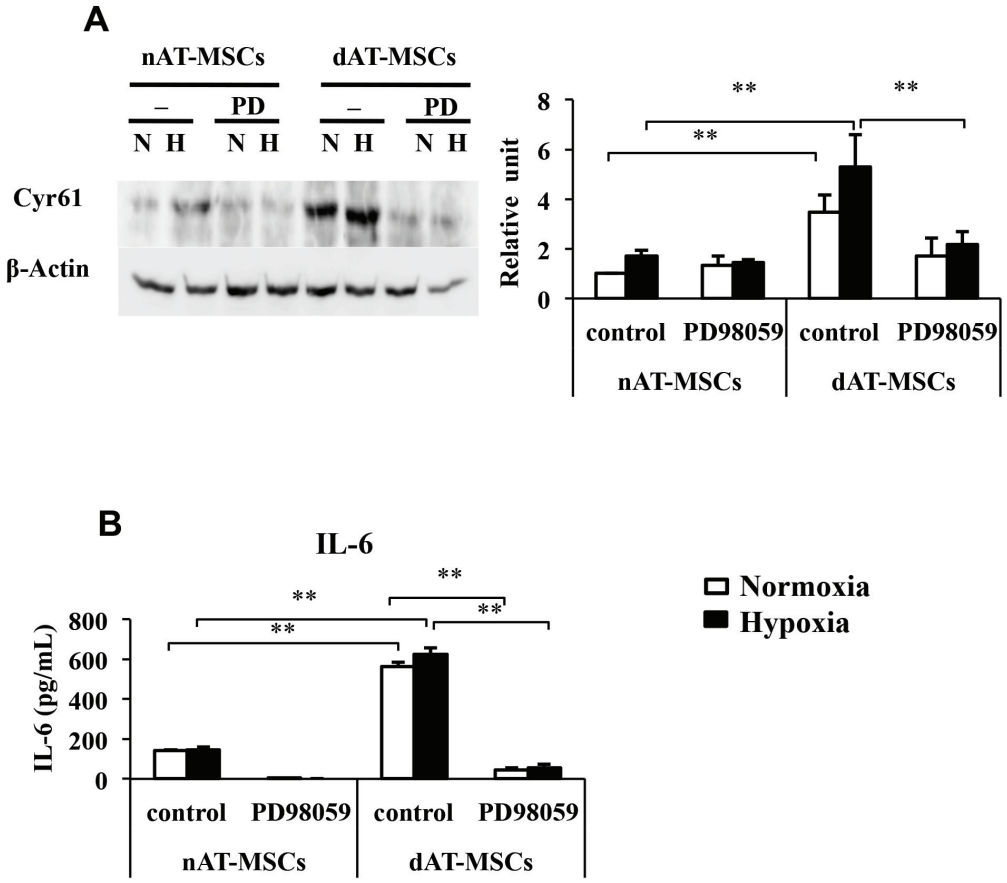

Fig. 10. The expression of Cyr61 and IL6 at protein levels in dAT-MSCs treated with inhibitor. PD98059 (50 μM) was added to nAT-MSC and dAT-MSC cultures for 60 min that were maintained under normoxic (20% O_2) or hypoxic (5% O_2) conditions. **A,** The protein levels of Cyr61 was examined by immunoblot analysis, and normalized to β-Actin. **B,** The quantitative protein concentration of IL-6 present in cell culture supernatants was measured by ELISA assay. The white and black bars indicate normoxic and hypoxic conditions, respectively. Controls representative for non-treated cells. The data shown are the averages of three independent experiments (mean ± SD). *, $P < 0.05$; **, $P < 0.01$.

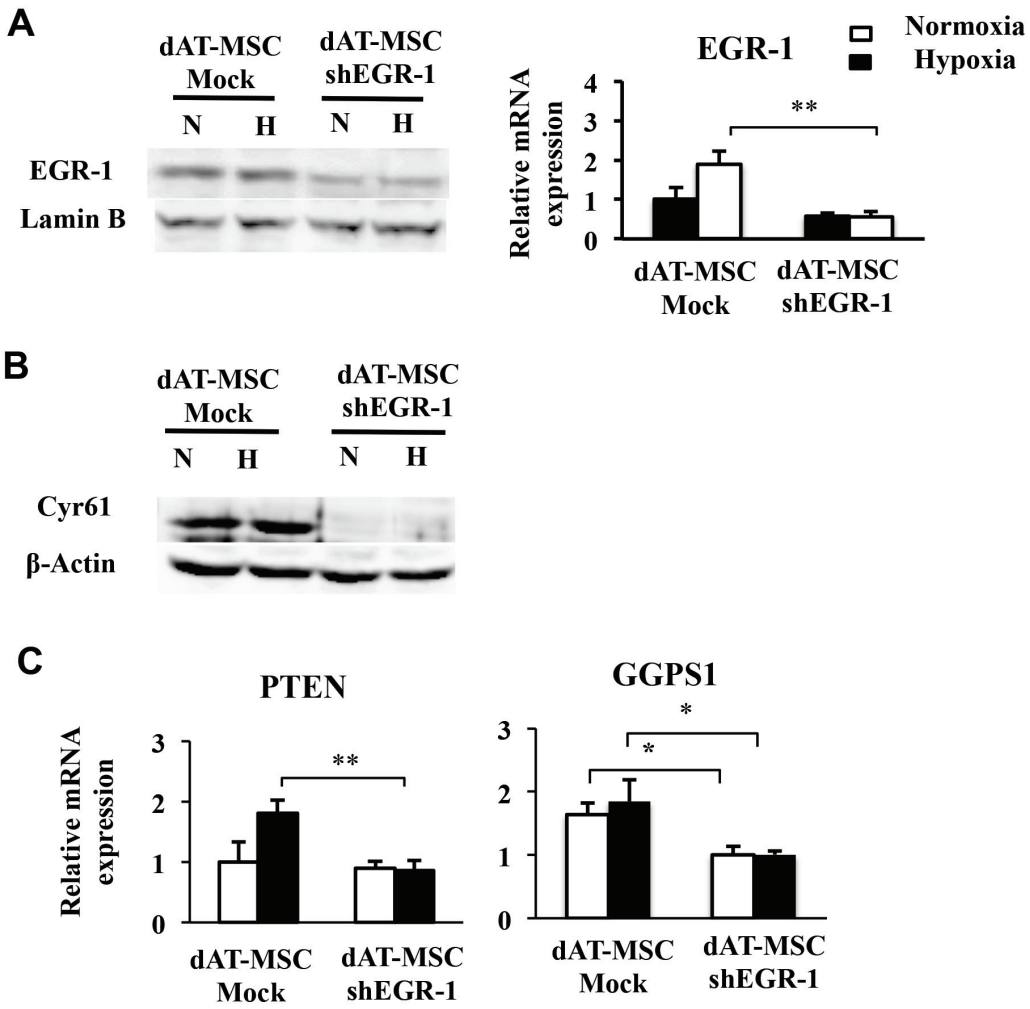

Fig. 11. Knock-down of EGR-1 decreased protein and genes related to cell adhesion and insulin resistance. A, dAT-MSCs were transfected with shRNA lentiviral transduction particles targeting EGR-1 (dAT-MSC-shEGR-1). The control cells were transfected with lentiviral control (dAT-MSC-Mock). After puromycin selection, the cells were cultured under normoxic (20% O_2) and hypoxic conditions (5% O_2) for 4 days. The mRNA and protein levels of EGR-1 were examined by a qRT-PCR and an immunoblot analysis, respectively. **B,** The protein levels of Cyr61 and the internal control β-Actin were assessed by immunoblot analysis. **C,** The mRNA expression levels of the EGR-1 target genes were assessed by a qPCR and normalized to β-Actin including PTEN and GGPS1. The white and black bars indicate normoxic and hypoxic conditions, respectively. The data represent the averages of three independent experiments (mean ± SD); *, $P < 0.05$, **, $P < 0.01$. N, normoxia; H, hypoxia.

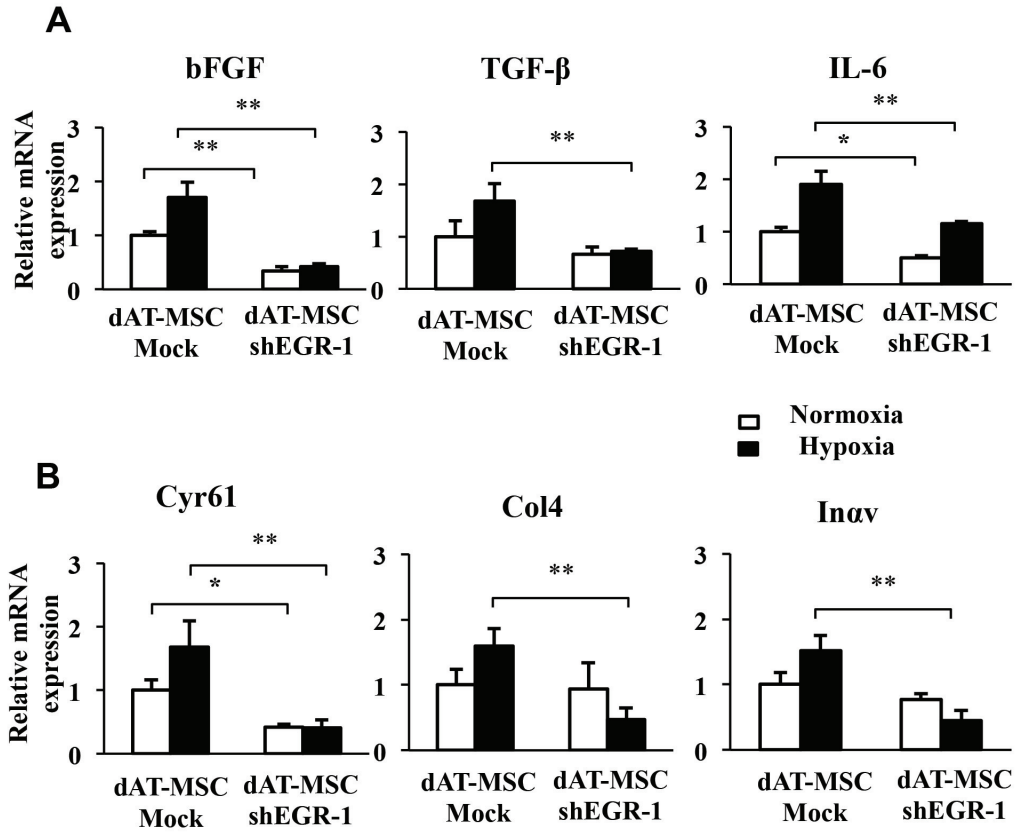

Fig. 12. The expression levels of genes related to cell proliferation, inflammation, and adhesion were down-regulated in dAT-MSCs with shEGR-1. A, dAT-MSCs were transfected with shRNA lentiviral transduction particles targeting EGR-1 (dAT-MSC-shEGR-1). The control cells were transfected with lentiviral control (dAT-MSC-Mock). After puromycin selection, the cells were cultured under normoxic (20% O_2) and hypoxic conditions (5% O_2) for 4 days. **A and B,** The mRNA expression levels of the EGR-1 target genes were assessed by a qPCR and normalized to β-Actin including bFGF, TGF-β, and IL-6 **(A)**; Cyr61, Col4, and Inαv **(B)**. The white and black bars indicate normoxic and hypoxic conditions, respectively. The data represent the averages of three independent experiments (mean ± SD); *, $P < 0.05$, **, $P < 0.01$.

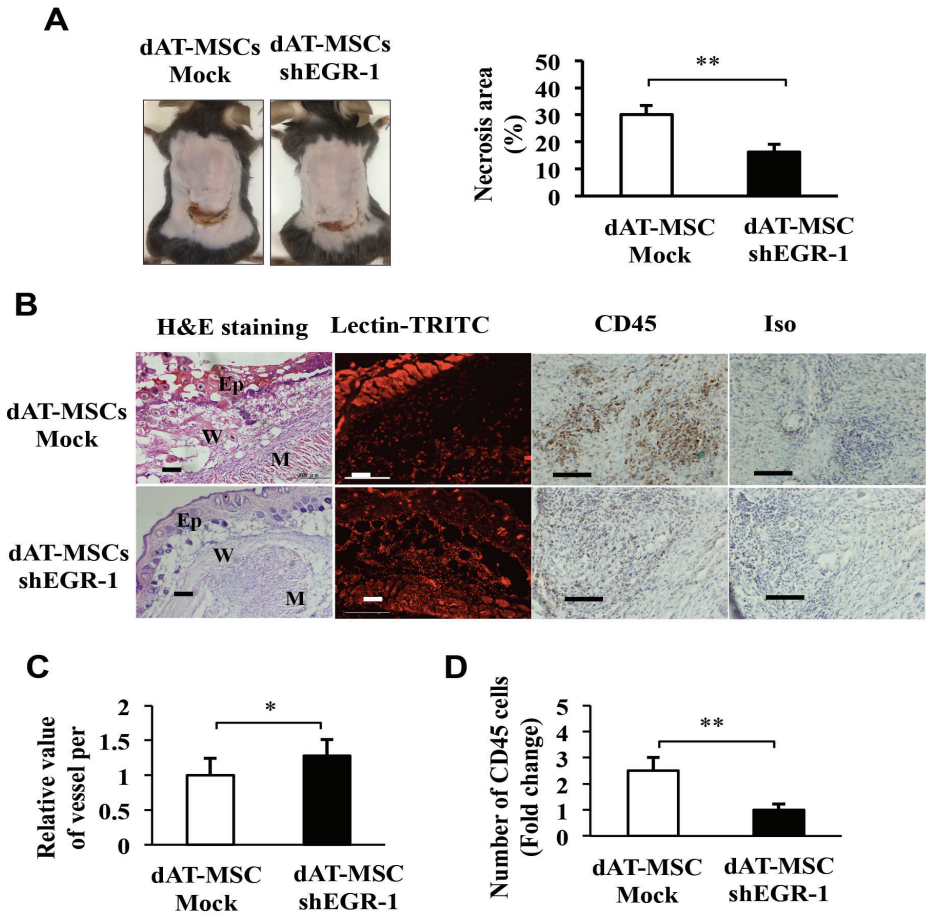

Fig. 13. Wound healing capacity was improved in dAT-MSC-shEGR-1 injected mice. A, Images of necrotic areas in mice that were injected dAT-MSC-mock and dAT-MSC-shEGR-1 were captured at day 7 after transplantation. The percentage of the necrotic area was calculated based on the area of necrotic tissue in relation to the wound area of mice injected with dAT-MSC-mock (n = 5) and dAT-MSC-shEGR-1 (n = 6). The knockdown of EGR-1 significantly increased the rate of wound healing in comparison to the control group. **B,** The embedded sections were examined by hematoxylin and eosin staining for tissue structure, which revealed the epidermis, wound, and muscle in each wound site; BI Lectin-TRITC staining was used to reveal the vessel formation (red); CD45 immunohistochemistry staining was performed to identify the inflammatory cells (brown). **C,** The activity of vessel formation in each area was measured based on fluorescence intensity using the Image J software program (n = 20). **D,** The number of CD45 positive cells were counted relative to the number of dAT-MSC-mock cells (n = 10). The data represent the average results from independent experiments (mean ± SD). *, $P < 0.05$; **, $P < 0.01$. Scale bars: 100μm; Ep, epidermis; W, wound; M, muscle.

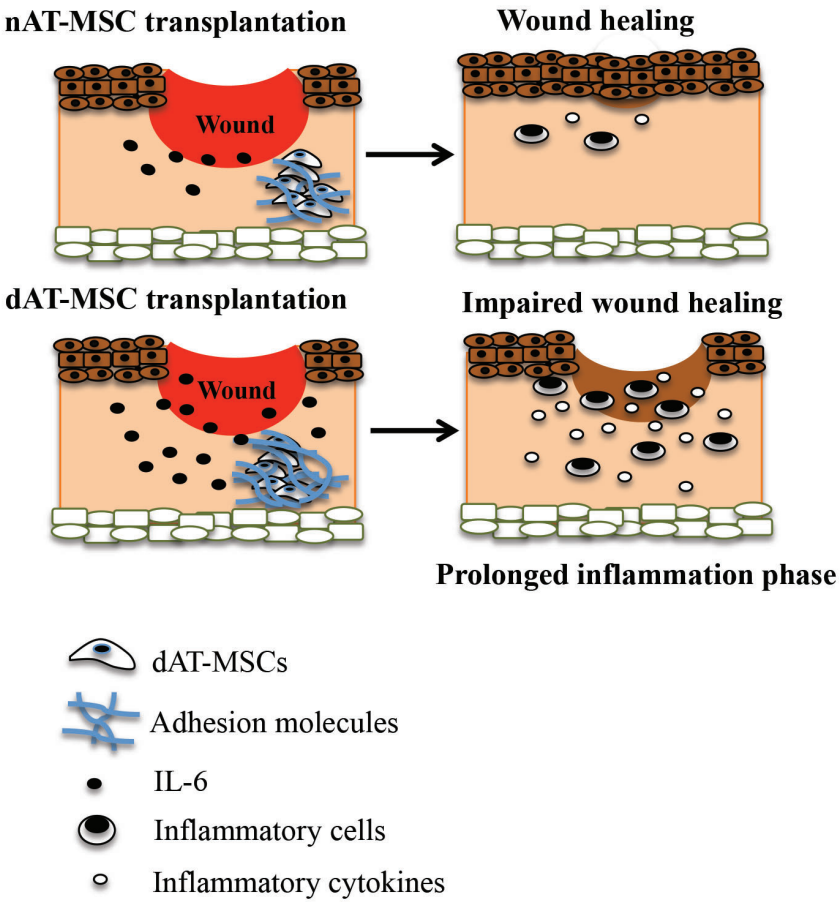

Fig. 14. A schematic illustration of wound healing process with nAT-MSC or dAT-MSC transplantation. The wound healing ability of dAT-MSCs was impaired due to adhesion molecules and excessive IL-6. This impairment might lead to a prolonged inflammation phase and delayed wound healing in comparison to the normal wound healing process with nAT-MSC transplantation.

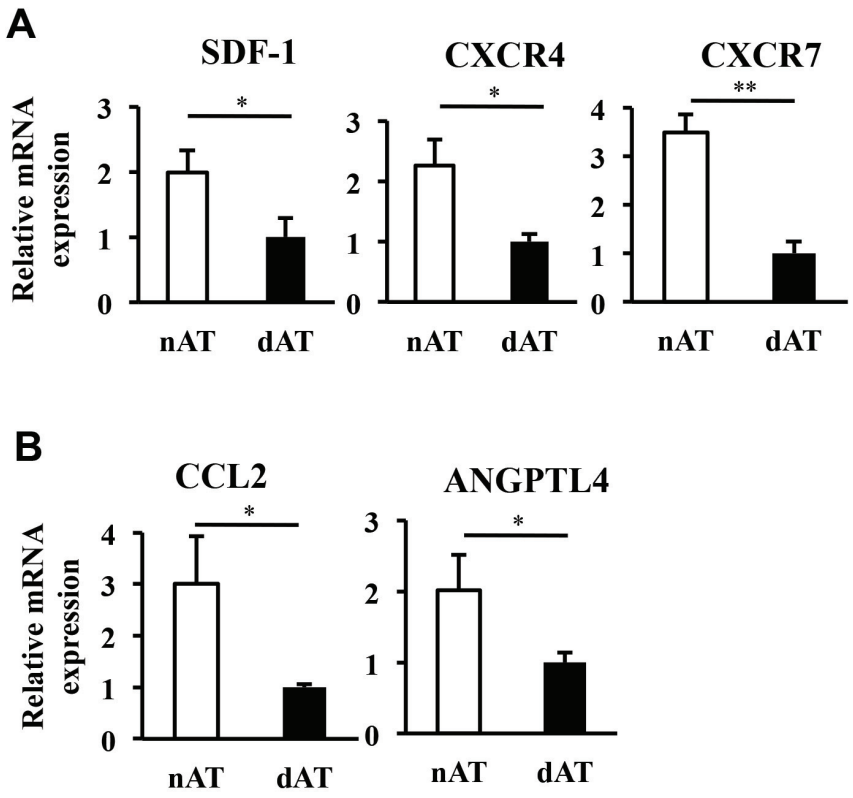

Fig. 15. The impairment of dAT-MSCs in gene expression associated with cell migration, inflammation, angiogenesis. A and B, The expression of genes) were evaluated in nAT-MSCs and dAT-MSCs by qRT-PCR and normalized to β-actin including SDF-1, CXCR4, and CXCR7 **(A)**; CCL2 and ANGPTL4 **(B)**. The data represent the averages of three independent experiments (mean ± SD); *, $P < 0.05$, **, $P < 0.01$.

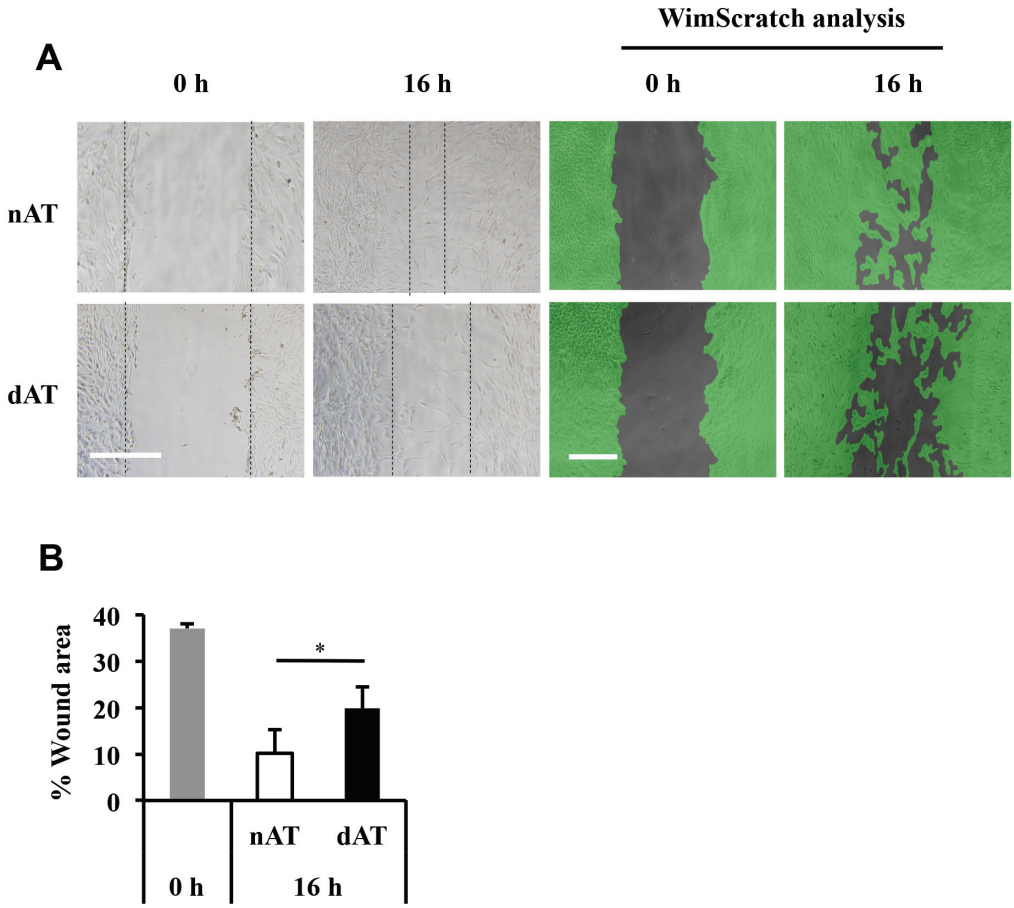

Fig. 16. The impairment of dAT-MSCs in wound healing in vitro. A, AT-MSCs were treated with mitomycin C for 3 h before the wound was scraped with a p1000 pipette tip to create a scratch (wound) in vitro (1 mm width). Representative images were captured by microscope and analyzed using the WimScratch software program (https://mywim.wimasis.com). **B,** The percentage of uncovered wound areas in nAT-MSCs and dAT-MSCs were analyzed at 0 h and 16 h. The presented data are the average of ten measurements from five dependent wounds. The data represent the averages of three independent experiments (mean ± SD); *, $P < 0.05$, **, $P < 0.01$. Scale bar: 500 µm

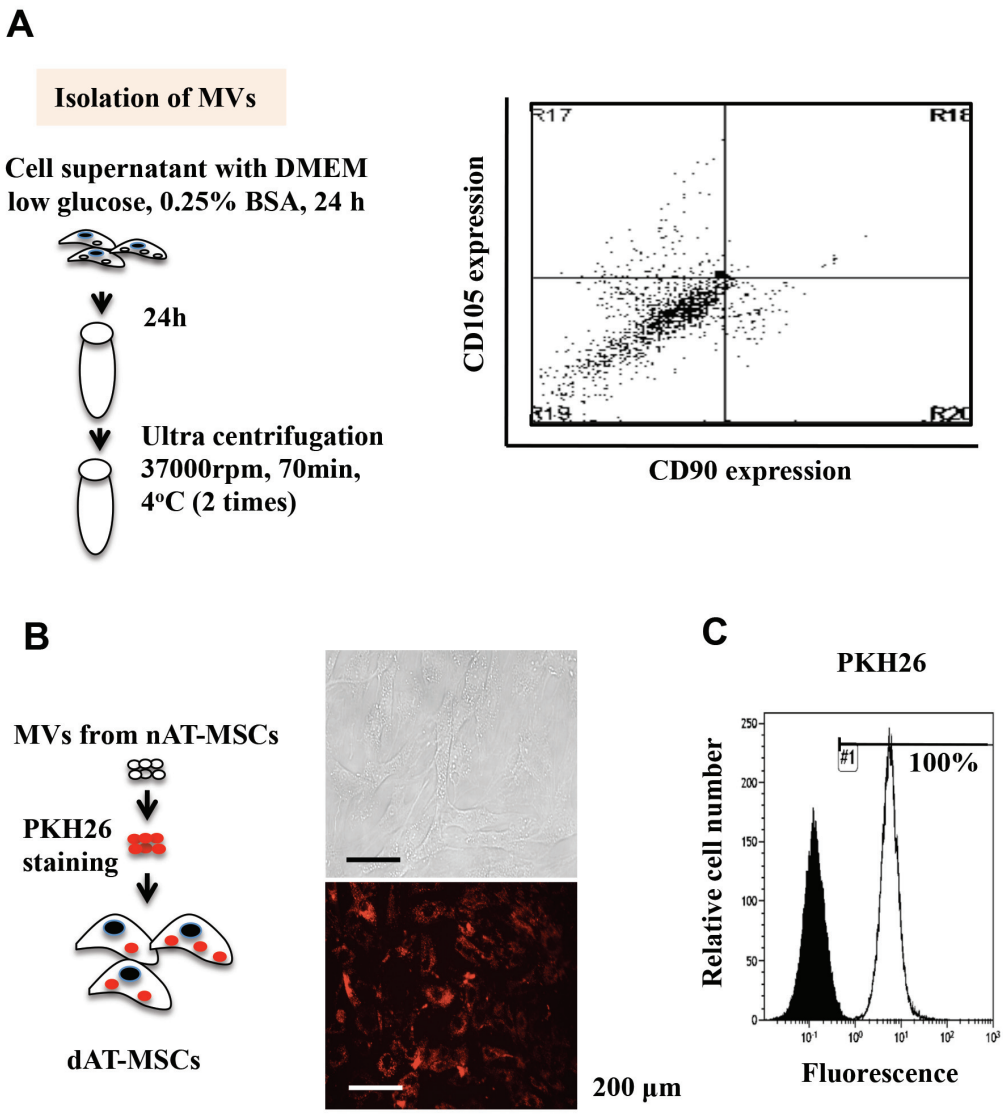

Fig. 17. nAT-MSC-derived MVs expressed mesenchymal stem cell surface markers and internalize into dAT-MSCs. A, MVs were analyzed and sorted by the FACS Vantage SE to determine the expressions of MSC surface markers CD105, CD90. **B,** Internalization ability of MVs into dAT-MSCs was examined under microscopy with red fluorescence by PKH26 staining. The images were taken after transfecting MVs at 12 h. **C,** Quantification of MVs transfected-dAT-MSCs according to the PKH26 red fluorescence signal was carried out using the FACS Vantage SE.

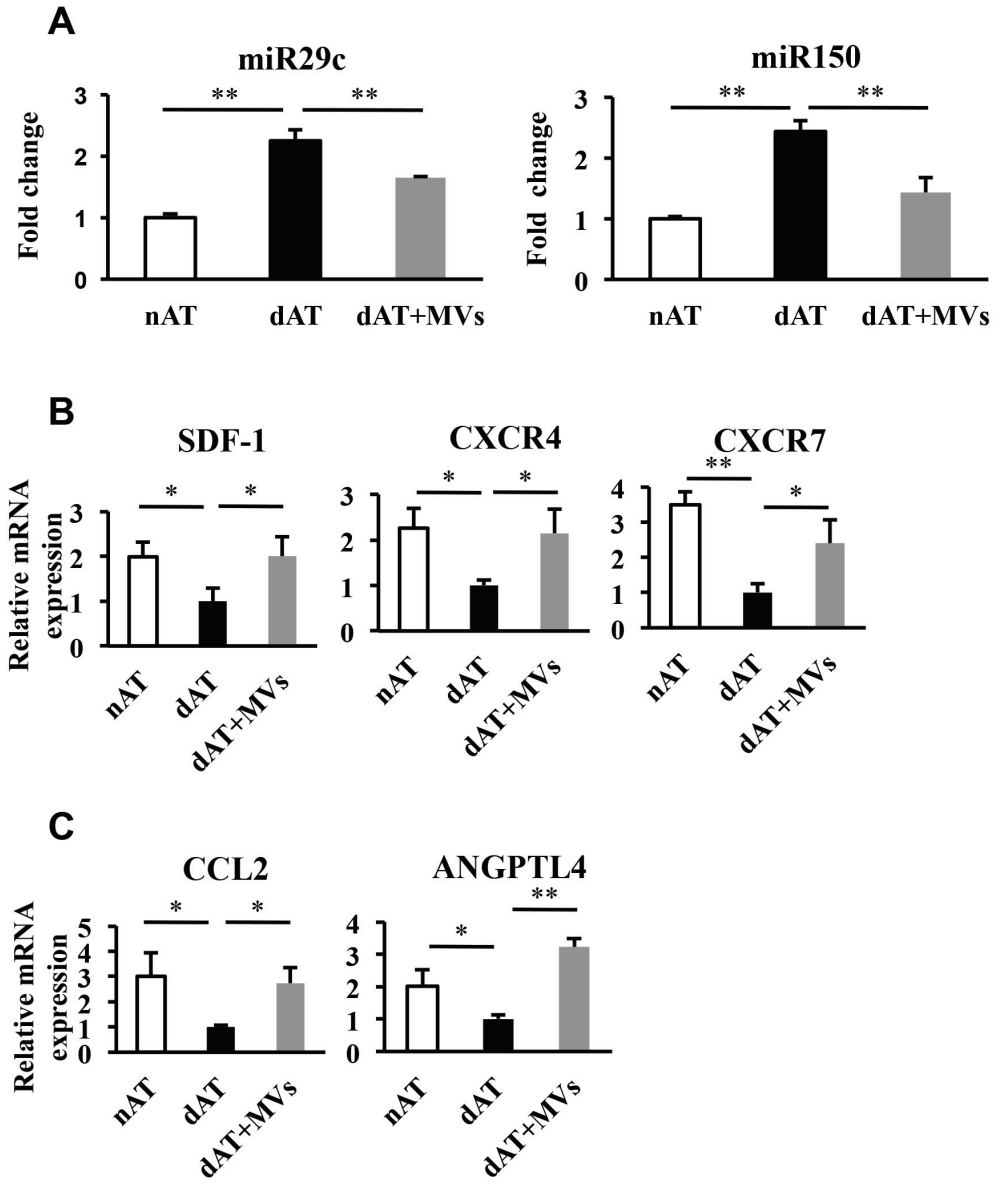

Fig. 18. nAT-MSC-derived MVs modulated the expression levels of miRNAs and mRNAs in MV-treated dAT-MSCs. **A,** The expression of miR29c and miR150 was examined by two-step RT-PCR and normalized to the endogenous control (RNU48). **B and C**, The expression of genes related to cell migration, survival, inflammation, and angiogenesis in nAT-MSCs, dAT-MSCs, and dAT-MSCs plus MVs, including SDF-1 and its receptors: CXCR4 and CXCR7 **(B)**; CCL2, ANGPTL4, and COL1A2 **(C)**. The expression of SDF-1, CXCR4, CXCR7, CCL2, and ANGPTL4 was decreased in dAT-MSCs and recovered in dAT-MSCs plus MVs. The data represent the average of three independent experiments (mean ± SD); *, $P < 0.05$; **, $P < 0.01$.

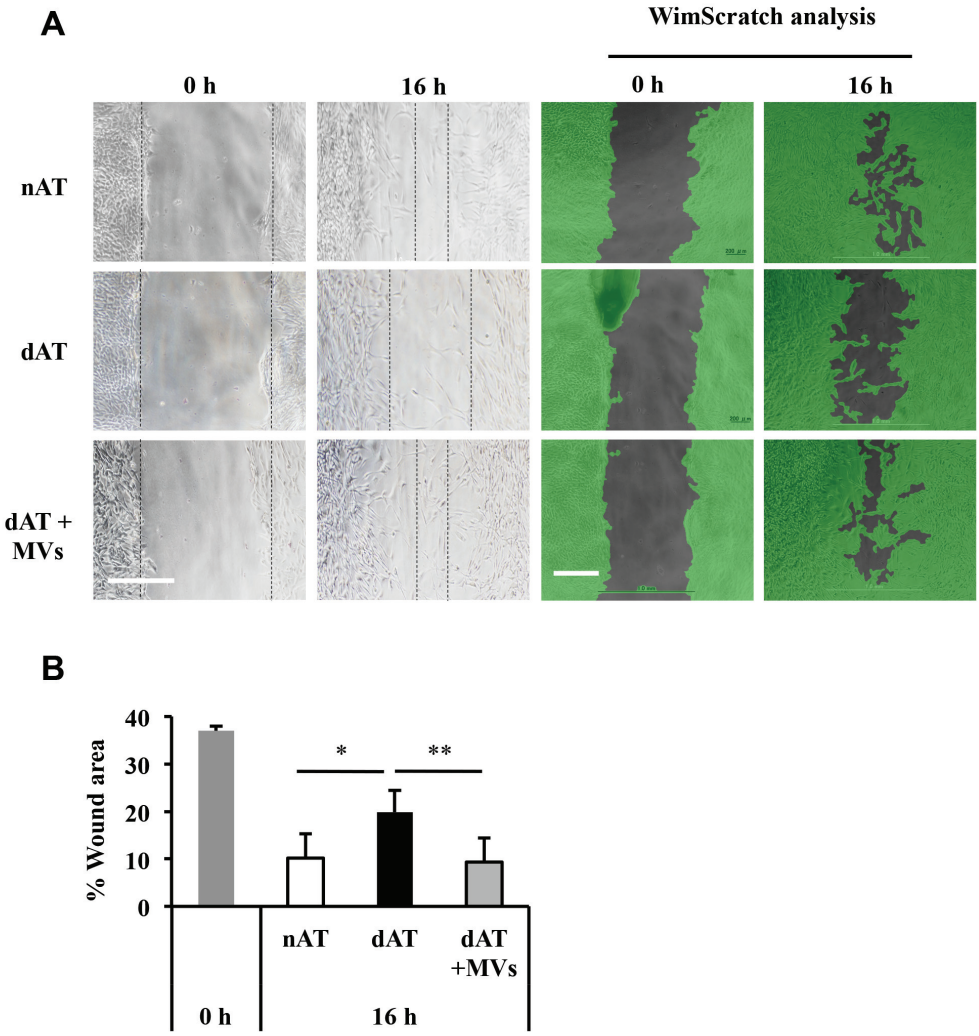

Fig. 19. nAT-MSC-derived MVs enhance wound healing ability of dAT-*MSCs in vitro.* nAT-MSC-derived MVs were transfected into dAT-MSCs and compared with the control (non-transfected cells) and nAT-MSCs. **A,** Representative images were captured by microscope and analyzed using the WimScratch software program (https://mywim.wimasis.com) at 0 h and 16 h. **B,** The percentage of uncovered wound areas from nAT-MSCs, dAT-MSCs, and MV-transfected dAT-MSCs at 0 h and 16 h. The data are the average of ten measurements from five dependent wounds (mean ± SD); *, $P < 0.05$; **, $P < 0.01$. Scale bars: 500 µm.

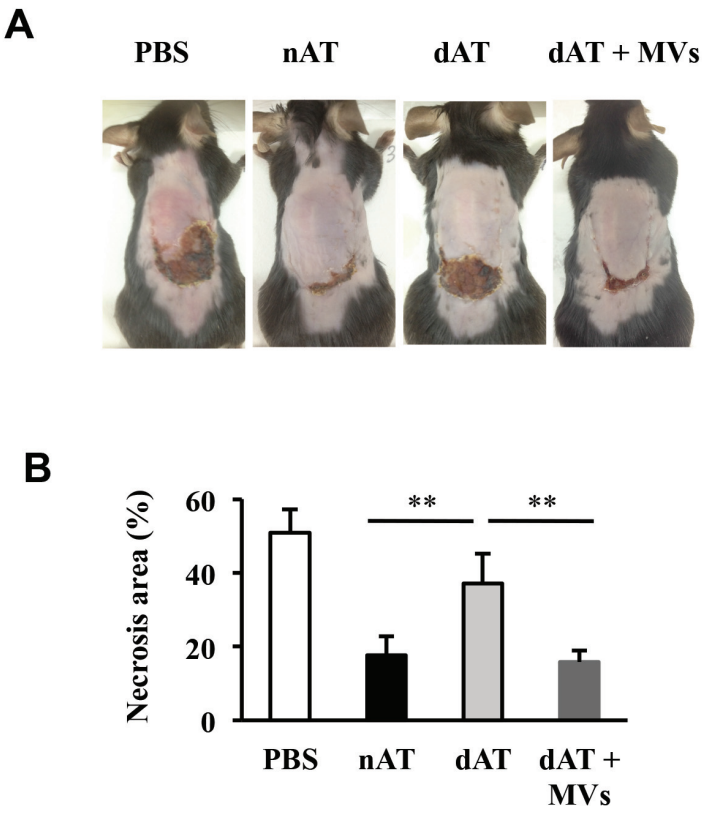

Fig. 20. MV-treated dAT-MSCs improved wound healing ability in the flap mouse model. A, Images of necrotic areas in mice injected with PBS, nAT-MSCs, and dAT-MSCs, or dAT-MSCs plus MVs were captured at day 7. **B,** The percentage of the necrotic area was calculated according to the necrotic area per wound area in mice. The data represent the average of three independent experiments (mean ± SD); *, $P < 0.05$; **, $P < 0.01$.

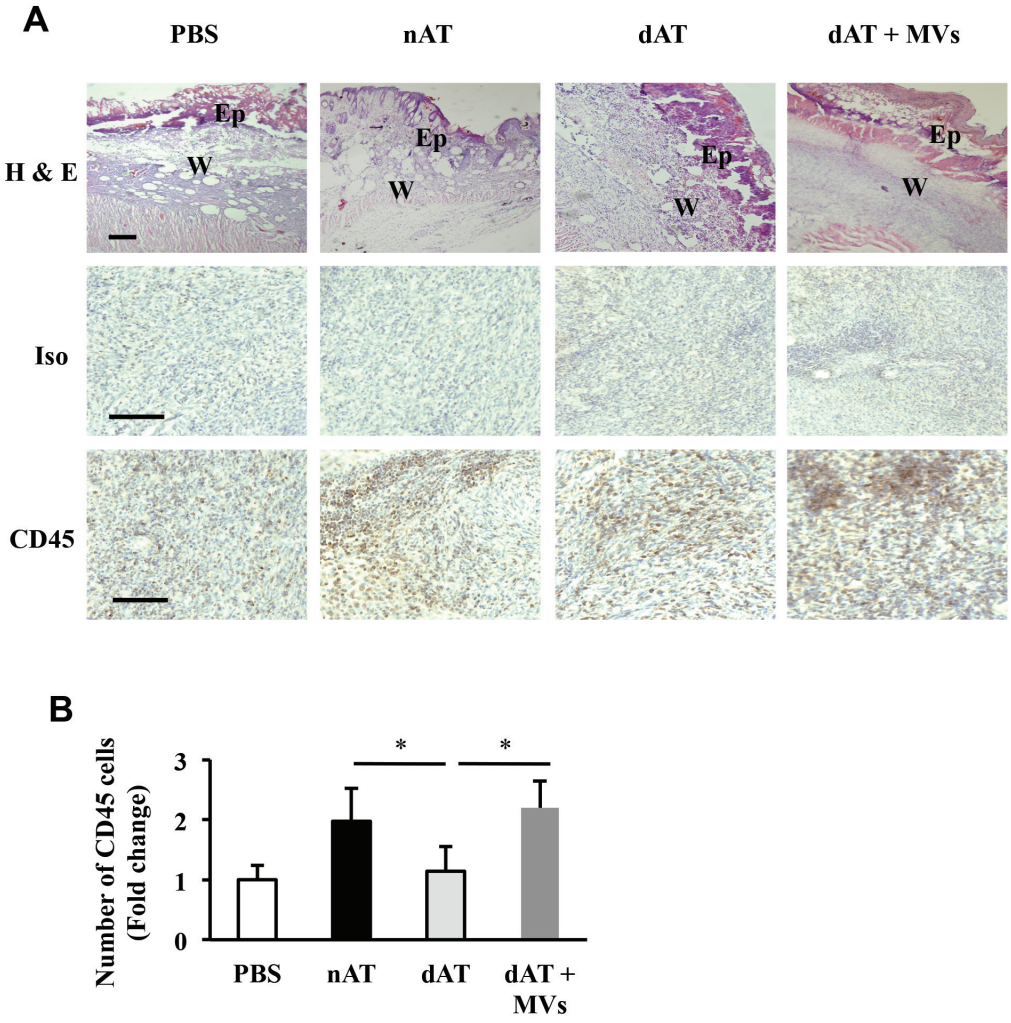

Fig. 21. Tissue structure and early response inflammation were enhanced in MV-treated dAT-MSC injected mice. The embedded sections were analyzed at day 3 of the flap mouse model. **A,** Hematoxylin and eosin was stained to examined tissue structure, which revealed the epidermis and wound areas in each wound site; CD45 immunohistochemical staining of inflammatory cells (brown). **B,** The numbers of CD45-positive cells were counted on three fields per stained section. The data present the fold change of CD45-positive cell number among groups. All data represent the average of three independent experiments (mean ± SD); *, $P < 0.05$; **, $P < 0.01$. Scale bars: 200 μm; Ep, epidermis; W, wound.

参　考　論　文

References

1. Vos T et al. (2015). Global, regional, and national incidence, prevalence, and years lived with disability for 301 acute and chronic diseases and injuries in 188 countries, 1990–2013: a systematic analysis for the Global Burden of Disease Study 2013. The Lancet 386:743-800.
2. Zimmet P, Alberti KG, Shaw J. (2001). Global and societal implications of the diabetes epidemic. Nature 414: 782–87.
3. Stumvoll M, BJ Goldstein and TW van Haeften. (2005). Type 2 diabetes: principles of pathogenesis and therapy. The Lancet 365:1333-1346.
4. Knudsen SH and BK Pedersen. (2015). Targeting Inflammation Through a Physical Active Lifestyle and Pharmaceuticals for the Treatment of Type 2 Diabetes. Curr Diab Rep 82: doi:10.1007/s11892-015-0642-1.
5. Barnett AH, B Charbonnel, RG Moses and S Kalra. (2015). Dipeptidyl peptidase-4 inhibitors in triple oral therapy regimens in patients with type 2 diabetes mellitus. Curr Med Res Opin 11:1-13.
6. Ryan GJ, LJ Jobe and R Martin. (2005). Pramlintide in the treatment of type 1 and type 2 diabetes mellitus. Clinical Therapeutics 27:1500-1512.
7. Brownlee M. (2001). Biochemistry and molecular cell biology of diabetic complications. Nature 414:813-820.
8. Alexandru N, E Badila, E Weiss, D Cochior, E Stępień and A Georgescu. (2016). Vascular complications in diabetes:

Microparticles and microparticle associated microRNAs as active players. Biochemical and Biophysical Research Communications 472:1-10.

9. Blakytny R and E Jude. (2006). The molecular biology of chronic wounds and delayed healing in diabetes. Diabet Med 23:594-608.
10. Gallagher KA, A Joshi, WF Carson, M Schaller, R Allen, S Mukerjee, N Kittan, EL Feldman, PK Henke, C Hogaboam, CF Burant and SL Kunkel. (2015). Epigenetic changes in bone marrow progenitor cells influence the inflammatory phenotype and alter wound healing in type 2 diabetes. Diabetes 64:1420-1430.
11. Brem H, Tomic-Canic M. Cellular and molecular basis of wound healing in diabetes. J Clin Invest. 2007; 117: 1219–22.
12. Bekker-Mendez C, RM Guzman-Aguilar, MA Hernandez-Cueto, S Huerta-Yepez, RA Jarillo-Luna, E Gonzalez-Veyrand and CR Gonzalez-Bonilla. (2012). TUNEL-positive cells in the surgical border of an amputation due to infected diabetic foot. Mol Med Rep 5:363-372.
13. Carreau A, BE Hafny-Rahbi, A Matejuk, C Grillon and C Kieda. (2011). Why is the partial oxygen pressure of human tissues a crucial parameter? Small molecules and hypoxia. Journal of Cellular and Molecular Medicine 15:1239-1253.
14. Girgis CM, K Cheng, CH Scott and JE Gunton. (2012). Novel links between HIFs, type 2 diabetes, and metabolic syndrome. Trends Endocrinol Metab 23:372-80.
15. Yan SF, N Mackman, W Kisiel, DM Stern and DJ Pinsky. (1999). Hypoxia/Hypoxemia-Induced activation of the procoagulant

pathways and the pathogenesis of ischemia-associated thrombosis. Arterioscler Thromb Vasc Biol 19:2029-2035.

16. Mavridis G, E Souliou, E Diza, G Symeonidis, F Pastore, AM Vassiliou and D Karamitsos. (2008). Inflammatory cytokines in insulin-treated patients with type 2 diabetes. Nutr Metab Cardiovasc Dis 18:471-476.
17. Elbarghati L, C Murdoch and CE Lewis. (2008). Effects of hypoxia on transcription factor expression in human monocytes and macrophages. Immunobiology 213:899-908.
18. Greer SN, JL Metcalf, Y Wang and M Ohh. (2012). The updated biology of hypoxia-inducible factor. EMBO J 31:2448-2460.
19. Semenza Gregg L. Hypoxia-Inducible Factors in Physiology and Medicine. Cell 148:399-408.
20. Yan SF, J Lu, YS Zou, J Soh-Won, DM Cohen, PM Buttrick, DR Cooper, SF Steinberg, N Mackman, DJ Pinsky and DM Stern. Hypoxia-associated induction of early growth response-1 gene expression. J Biol Chem 1999 274:15030-40.
21. Yan S-F, T Fujita, J Lu, K Okada, Y Shan Zou, N Mackman, DJ Pinsky and DM Stern. (2000). Egr-1, a master switch coordinating upregulation of divergent gene families underlying ischemic stress. Nat Med 6:1355-1361.
22. Sukhatme VP, Cao XM, Chang LC, Tsai-Morris CH, Stamenkovich D, Ferreira PC, Cohen DR, Edward SA, Shows TB, Curran T, Le Beau MM, Adamson ED. A zinc finger-encoding gene coregulated with c-fos during growth and differentiation, and after cellular depolarization. Cell 1988;53:37–43.

23. Khachigian LM. (2006). Early growth response-1 in cardiovascular pathobiology. Circ Res 98:186-191
24. Kim JN, HJ Kim, SH Jeong, YC Kye and SW Son. (2011). Cigarette smoke-induced early growth response-1 regulates the expression of the cysteine-rich 61 in human skin dermal fibroblasts. Exp Dermatol 20:992-997.
25. Harja E, LG Bucciarelli, Y Lu, DM Stern, YS Zou, AM Schmidt and S-F Yan. (2004). Early Growth Response-1 Promotes Atherogenesis: Mice Deficient in Early Growth Response-1 and Apolipoprotein E Display Decreased Atherosclerosis and Vascular Inflammation. Circ Res 94:333-339.
26. Yu X, N Shen, M-L Zhang, F-Y Pan, C Wang, W-P Jia, C Liu, Q Gao, X Gao, B Xue and C-J Li. (2011). Egr-1 decreases adipocyte insulin sensitivity by tilting PI3K/Akt and MAPK signal balance in mice. EMBO J 30:3754-3765.
27. Shen N, X Yu, F-Y Pan, X Gao, B Xue and C-J Li. (2011). An Early Response Transcription Factor, Egr-1, Enhances Insulin Resistance in Type 2 Diabetes with Chronic Hyperinsulinism. Journal of Biological Chemistry 286:14508-14515.
28. Zuk PA, M Zhu, H Mizuno, J Huang, JW Futrell, AJ Katz, P Benhaim, HP Lorenz and MH Hedrick. (2001). Multilineage cells from human adipose tissue: implications for cell-based therapies. Tissue Eng 7:211-228.
29. Zuk PA, M Zhu, P Ashjian, DA De Ugarte, JI Huang, H Mizuno, ZC Alfonso, JK Fraser, P Benhaim and MH Hedrick. (2002). Human adipose tissue is a source of multipotent stem cells. Mol Biol Cell

13:4279-95.

30. Gaiba S, LP Franca, JP Franca and LM Ferreira. (2012). Characterization of human adipose-derived stem cells. Acta Cir Bras 27:471-6.
31. Finesmith TH, KN Broadley and JM Davidson. (1990). Fibroblasts from wounds of different stages of repair vary in their ability to contract a collagen gel in response to growth factors. J Cell Physiol 144:99-107.
32. Jackson WM, LJ Nesti and RS Tuan. (2012). Concise review: clinical translation of wound healing therapies based on mesenchymal stem cells. Stem Cells Transl Med 1:44-50.
33. Akimoto K, K Kimura, M Nagano, S Takano, G To'a Salazar, T Yamashita and O Ohneda. (2013). Umbilical cord blood-derived mesenchymal stem cells inhibit, but adipose tissue-derived mesenchymal stem cells promote, glioblastoma multiforme proliferation. Stem Cells Dev 22:1370-86.
34. Gao W, X Qiao, S Ma and L Cui. (2011). Adipose-derived stem cells accelerate neovascularization in ischaemic diabetic skin flap via expression of hypoxia-inducible factor-1alpha. J Cell Mol Med 15:2575-85.
35. Minteer D, K Marra and JP Rubin. (2012). Adipose-Derived Mesenchymal Stem Cells: Biology and Potential Applications. Springer Berlin Heidelberg. pp 1-13.
36. Kimura K, M Nagano, G Salazar, T Yamashita, I Tsuboi, H Mishima, S Matsushita, F Sato, K Yamagata and O Ohneda. (2014). The role of CCL5 in the ability of adipose tissue-derived

mesenchymal stem cells to support repair of ischemic regions. Stem Cells Dev 23:488-501.

37. Cramer C, E Freisinger, RK Jones, DP Slakey, CL Dupin, ER Newsome, EU Alt and R Izadpanah. (2010). Persistent high glucose concentrations alter the regenerative potential of mesenchymal stem cells. Stem Cells Dev 19:1875-1884.
38. Nagano M, T Yamashita, H Hamada, K Ohneda, K-i Kimura, T Nakagawa, M Shibuya, H Yoshikawa and O Ohneda. (2007). Identification of functional endothelial progenitor cells suitable for the treatment of ischemic tissue using human umbilical cord blood. Blood 110:151-160.
39. Tontonoz P, RA Graves, AI Budavari, H Erdjument-Bromage, M Lui, E Hu, P Tempst and BM Spiegelman. (1994). Adipocyte-specific transcription factor ARF6 is a heterodimeric complex of two nuclear hormone receptors, PPAR gamma and RXR alpha. Nucleic Acids Res 22:5628-5634.
40. Diez JJ and P Iglesias. (2003). The role of the novel adipocyte-derived hormone adiponectin in human disease. Eur J Endocrinol 148:293-300.
41. Lee KS, HJ Kim, QL Li, XZ Chi, C Ueta, T Komori, JM Wozney, EG Kim, JY Choi, HM Ryoo and SC Bae. (2000). Runx2 is a common target of transforming growth factor beta1 and bone morphogenetic protein 2, and cooperation between Runx2 and Smad5 induces osteoblast-specific gene expression in the pluripotent mesenchymal precursor cell line C2C12. Mol Cell Biol 20:8783-8792.

42. Farley JR, JE Wergedal and DJ Baylink. (1983). Fluoride directly stimulates proliferation and alkaline phosphatase activity of bone-forming cells. Science 222:330-332.

43. Von Bauer R, D Oikonomou, A Sulaj, S Mohammed, A Hotz-Wagenblatt, H-J Gröne, B Arnold, C Falk, D Luethje, A Erhardt, DM Stern, A Bierhaus and PP Nawroth. (2013). CD166/ALCAM Mediates Proinflammatory Effects of S100B in Delayed Type Hypersensitivity. In: The Journal of Immunology. pp 369-377.

44. Yan SF, R Ramasamy and AM Schmidt. (2008). Mechanisms of Disease: advanced glycation end-products and their receptor in inflammation and diabetes complications. Nat Rev Endocrinol 4:285-293.

45. Bouzakri K, M Roques, P Gual, S Espinosa, F Guebre-Egziabher, J-P Riou, M Laville, Y Le Marchand-Brustel, J-F Tanti and H Vidal. (2003). Reduced Activation of Phosphatidylinositol-3 Kinase and Increased Serine 636 Phosphorylation of Insulin Receptor Substrate-1 in Primary Culture of Skeletal Muscle Cells From Patients With Type 2 Diabetes. Diabetes 52:1319-1325.

46. Sun XJ, P Rothenberg, CR Kahn, JM Backer, E Araki, PA Wilden, DA Cahill, BJ Goldstein and MF White. (1991). Structure of the insulin receptor substrate IRS-1 defines a unique signal transduction protein. Nature 352:73-77.

47. Olefsky JM. (1976). The Insulin Receptor: Its Role in Insulin Resistance of Obesity and Diabetes. Diabetes 25:1154-1161.

48. Deindl J-IPaE. (2012). Disease Progression Mediated by Egr-1 Associated Signaling in Response to Oxidative Stress. Int J Mol Sci 13:13104–13117.

49. Chen S-J, H Ning, W Ishida, S Sodin-Semrl, S Takagawa, Y Mori and J Varga. (2006). The Early-Immediate Gene EGR-1 Is Induced by Transforming Growth Factor-β and Mediates Stimulation of Collagen Gene Expression. J Biol Chem 281:21183-21197.

50. Bhattacharyya S, SJ Chen, M Wu, M Warner-Blankenship, H Ning, G Lakos, Y Mori, E Chang, C Nihijima, K Takehara, C Feghali-Bostwick and J Varga. (2008). Smad-independent transforming growth factor-beta regulation of early growth response-1 and sustained expression in fibrosis: implications for scleroderma. Am J Pathol 173:1085-1099.

51. Lee CG, SJ Cho, MJ Kang, SP Chapoval, PJ Lee, PW Noble, T Yehualaeshet, B Lu, RA Flavell, J Milbrandt, RJ Homer and JA Elias. (2004). Early growth response gene 1-mediated apoptosis is essential for transforming growth factor beta1-induced pulmonary fibrosis. J Exp Med 200:377-389.

52. Fahmy RG, CR Dass, LQ Sun, CN Chesterman and LM Khachigian. (2003). Transcription factor Egr-1 supports FGF-dependent angiogenesis during neovascularization and tumor growth. Nat Med 9:1026-32.

53. Gregg J and G Fraizer. (2011). Transcriptional Regulation of EGR1 by EGF and the ERK Signaling Pathway in Prostate Cancer Cells. Genes Cancer 2:900-9.

54. Lo LW, JJ Cheng, JJ Chiu, BS Wung, YC Liu and DL Wang. (2001). Endothelial exposure to hypoxia induces Egr-1 expression involving PKCalpha-mediated Ras/Raf-1/ERK1/2 pathway. J Cell Physiol 188:304-12.

55. You JJ, CH Yang, MS Chen and CM Yang. (2009). Cysteine-rich 61, a Member of the CCN Family, as a Factor Involved in the Pathogenesis of Proliferative Diabetic Retinopathy. Invest Ophthal & Vis Sci 50:3447-3455.

56. Doi T, A Mima, T Matsubara, T Tominaga, H Arai and H Abe. (2008). The current clinical problems for early phase of diabetic nephropathy and approach for pathogenesis of diabetic nephropathy. Diabetes Res Clin Pract 13:7.

57. Hayashi Y, H Makino and Z Ota. (1992). Serum and urinary concentrations of type IV collagen and laminin as a marker of microangiopathy in diabetes. Diabet Med 9:366-370.

58. Zhou D, DJ Herrick, J Rosenbloom and B Chaqour. (2005). Cyr61 mediates the expression of VEGF, αv-integrin, and α-actin genes through cytoskeletally based mechanotransduction mechanisms in bladder smooth muscle cells. Journal of Applied Physiology 98:2344-2354.

59. Zhu X, Y Song, R Huo, J Zhang, S Sun, Y He, H Gao, M Zhang, X Sun, T Zhai, H Li, Y Sun, Z Zhou, B Shen, L Xiao and N Li. (2015). Cyr61 participates in the pathogenesis of rheumatoid arthritis by promoting proIL-1beta production by fibroblast-like synoviocytes through an AKT-dependent NF-kappaB signaling pathway. Clin Immunol 157:187-97.

60. Mauer J, B Chaurasia, J Goldau, MC Vogt, J Ruud, KD Nguyen, S Theurich, AC Hausen, J Schmitz, HS Bronneke, E Estevez, TL Allen, A Mesaros, L Partridge, MA Febbraio, A Chawla, FT Wunderlich and JC Bruning. (2014). Signaling by IL-6 promotes alternative activation of macrophages to limit endotoxemia and obesity-associated resistance to insulin. Nat Immunol 15:423-430.
61. Fontes JA, NR Rose and D Cihakova. (2015). The varying faces of IL-6: From cardiac protection to cardiac failure. Cytokine 74:62-68.
62. Hossain M, MO Faruque, G Kabir, N Hassan, D Sikdar, Q Nahar and L Ali. (2010). Association of serum TNF-α and IL-6 with insulin secretion and insulin resistance in IFG and IGT subjects in a Bangladeshi population. Int J Diabetes Mellitus 2:165-168.
63. Liechty KW, NS Adzick and TM Crombleholme. (2000). Diminished interleukin 6 (IL-6) production during scarless human fetal wound repair. Cytokine 12:671-676.
64. Raposo G and W Stoorvogel. (2013). Extracellular vesicles: Exosomes, microvesicles, and friends. The Journal of Cell Biology 200:373-383.
65. De Luca L, S Trino, V Simeon, I Laurenzana, S Raimondo, M Podestà, M Santodirocco, L Di Mauro, F La Rocca, A Caivano, A Morano, L Del Vecchio, F Frassoni, D Cilloni and P Musto. (2014). Exposure of Cord Blood Hematopoietic Stem Cells to Bone Marrow Mesenchimal Cells-Derived Microvesicles Induces Cell Survival and Inhibition of Differentiation. Blood 124:4364-4364.
66. Sabin K and N Kikyo. (2014). Microvesicles as mediators of tissue regeneration. Translational Research 163:286-295.

67. Collino F, MC Deregibus, S Bruno, L Sterpone, G Aghemo, L Viltono, C Tetta and G Camussi. (2010). Microvesicles Derived from Adult Human Bone Marrow and Tissue Specific Mesenchymal Stem Cells Shuttle Selected Pattern of miRNAs. PLoS ONE 5:e11803.
68. Gatti S, S Bruno, MC Deregibus, A Sordi, V Cantaluppi, C Tetta and G Camussi. (2011). Microvesicles derived from human adult mesenchymal stem cells protect against ischaemia–reperfusion-induced acute and chronic kidney injury. Nephrology Dialysis Transplantation.
69. Sdrimas K and S Kourembanas. (2014). MSC Microvesicles for the Treatment of Lung Disease: A New Paradigm for Cell-Free Therapy. Antioxidants & Redox Signaling 21:1905-1915.
70. Camussi G, Maria C Deregibus and V Cantaluppi. (2013). Role of stem-cell-derived microvesicles in the paracrine action of stem cells. Biochemical Society Transactions 41:283-287.
71. Monsel A, Y-g Zhu, S Gennai, Q Hao, S Hu, J-J Rouby, M Rosenzwajg, MA Matthay and JW Lee. (2015). Therapeutic Effects of Human Mesenchymal Stem Cell–derived Microvesicles in Severe Pneumonia in Mice. American Journal of Respiratory and Critical Care Medicine 192:324-336.
72. Favaro E, A Carpanetto, S Lamorte, A Fusco, C Caorsi, MC Deregibus, S Bruno, A Amoroso, M Giovarelli, M Porta, PC Perin, C Tetta, G Camussi and MM Zanone. (2014). Human mesenchymal stem cell-derived microvesicles modulate T cell response to islet antigen glutamic acid decarboxylase in patients with type 1 diabetes. Diabetologia 57:1664-1673.

73. Tu TC, M Nagano, T Yamashita, H Hamada, K Ohneda, K Kimura and O Ohneda. (2015). A Chemokine Receptor, CXCR4, Which Is Regulated by Hypoxia-Inducible Factor 2α, Is Crucial for Functional Endothelial Progenitor Cells Migration to Ischemic Tissue and Wound Repair. Stem Cells and Development 25:266-276.
74. Liang CC, AY Park and JL Guan. (2007). In vitro scratch assay: a convenient and inexpensive method for analysis of cell migration in vitro. Nat. Protocols 2:329-333.
75. Shabbir A, A Cox, L Rodriguez-Menocal, M Salgado and EV Badiavas. (2015). Mesenchymal Stem Cell Exosomes Induce Proliferation and Migration of Normal and Chronic Wound Fibroblasts, and Enhance Angiogenesis In Vitro. Stem Cells and Development 24:1635-1647.
76. Arya AK, K Tripathi and P Das. (2014). Promising role of ANGPTL4 gene in diabetic wound healing. Int J Low Extrem Wounds 13:58-63.
77. Liu H, S Liu, Y Li, X Wang, W Xue, G Ge and X Luo. (2012). The role of SDF-1-CXCR4/CXCR7 axis in the therapeutic effects of hypoxia-preconditioned mesenchymal stem cells for renal ischemia/reperfusion injury. PLoS ONE 7:12.
78. Zou X, G Zhang, Z Cheng, D Yin, T Du, G Ju, S Miao, G Liu, M Lu and Y Zhu. (2014). Microvesicles derived from human Wharton's Jelly mesenchymal stromal cells ameliorate renal ischemia-reperfusion injury in rats by suppressing CX3CL1. Stem Cell Research & Therapy 5:1-13.

79. He A, L Zhu, N Gupta, Y Chang and F Fang. (2007). Overexpression of Micro Ribonucleic Acid 29, Highly Up-Regulated in Diabetic Rats, Leads to Insulin Resistance in 3T3-L1 Adipocytes. Molecular Endocrinology 21:2785-2794.
80. Tano N, HW Kim and M Ashraf. (2011). microRNA-150 regulates mobilization and migration of bone marrow-derived mononuclear cells by targeting Cxcr4. PLoS ONE 6:19.
81. Tano N, KH Haider, HW Kim and M Ashraf. (2011). miR-150 regulates CXCR4 expression on bone marrow stem/progenitor cells for their mobilization and homing into the heart during acute phase of myocardial ischemia. The FASEB Journal 25:512.5.
82. Willeit P, A Zampetaki, K Dudek, D Kaudewitz, A King, NS Kirkby, R Crosby-Nwaobi, M Prokopi, I Drozdov, SR Langley, S Sivaprasad, HS Markus, JA Mitchell, TD Warner, S Kiechl and M Mayr. (2013). Circulating microRNAs as novel biomarkers for platelet activation. Circ Res 112:595-600.

Acknowledgments

I sincerely express my gratitude to my advisor, professor Osamu Ohneda, for providing me the opportunity to pursue my Master and Doctoral degrees in University of Tsukuba. I always appreciate your constructive criticism, valuable advice, and kind supports. You always encourage me to think and conduct research independently, which help me confident to become an independent researcher in the future.

I would like to thank Dr. Duong Hoa Xo, the director of Biotechnology center in Ho Chi Minh city–Vietnam, for giving me the opportunities to study and to accomplish my Master and Doctoral degree in University of Tsukuba.

To fulfill this dissertation, I would like to thank the thesis committee members, professor Akira Shibuya and three assistant professors: Dr. Ken Nishimura, Dr. Majime Mishima, and Dr. Kenji Yamagata for your kind comments and important advice.

I would like to thank Dr. Toshiharu Yamashita and Dr. Mami Matsuo-Takahashi for your kind instructions and supports to help improving my research.

I also thank Dr. Kenichi Kimura and Dr. Georgina To'a Salazar for guiding, encouraging and helping me from the very first days.

I greatly appreciate to all members in Prof. Ohneda's Laboratory for your friendship and kind supports. I always keep in mind the wonderful time we have had together for our Lab's activities. I am grateful to Ms. Tran Cam Tu for being more like a sister to me. You always give me hearty encouragement and advice for my study and life. You also help me enjoy my

time in Tsukuba by taking many beautiful and meaningful photos of my family.

I also would like to thank my Vietnamese and international friends who give me help and encouragement to make my stay in Japan enjoyable, valuable, and unforgettable.

I would like to express my sincere appreciation to Japanese Government MEXT Scholarship and Mitsubishi Foundation Scholarship for supporting my study and life in Tsukuba.

I would like to thank the members of the International office, Medical department office, and Academic Service Office for the Medical Science Area in University of Tsukuba for providing information and kind supports.

Finally, I truly express my gratitude to all members of my families, especially to my father, Trinh Van Hoang, and my mother, Nguyen Thi Kim Cuong, for giving me your endless love and unconditional help. I am very grateful to my beloved husband, Vong Binh Long, for all your love, encouragement, and assistance. With you and our son, Vong Quan Bao, by my side, I feel great joy and motivation for my study and life.

University of Tsukuba, 2016 July 12nd

Trinh Nhu Thuy

Published papers

Trinh Nhu Thuy, Yamashita T, Ohneda K, Kimura K, Salazar GTa, Sato F, Ohneda O. (2016). Increased Expression of EGR-1 in Diabetic Human Adipose Tissue-Derived Mesenchymal Stem Cells Reduces Their Wound Healing Capacity. *Stem Cells and Development* 25**:** 760-773

Trinh Nhu Thuy, Yamashita T, Tu TC, Kato T, Ohneda K, Sato F, Ohneda O. (2016). Microvesicles enhance the mobility of human diabetic adipose tissue-derived mesenchymal stem cells in vitro and improve wound healing in vivo. *Biochemical and Biophysical Research Communications* 473**:** 1111-1118